Research Paper

Anti-DNA virus agent cidofovir - loaded green synthesized cerium oxide nanoparticles (Nanoceria): Nucleic acids (DNA and RNA) binding affinity and cytotoxicity effects

Nahid Shahabadi¹, Saba Zendehcheshm¹, Fatemeh Khademi² and Mohammad Mahdavi¹

Correspondence to: Nahid Shahabadi, email: nahidshahabadi@yahoo.com, https://orcid.org/0009-0006-2687-3231

Keywords: CeO₂ NPs; green synthesis; DNA interaction; RNA interaction; cytotoxicity

Received: March 09, 2025 Accepted: September 30, 2025 Published: November 06, 2025

Copyright: © 2025 Shahabadi et al. This is an open access article distributed under the terms of the <u>Creative Commons Attribution</u> <u>License</u> (CC BY 4.0), which permits unrestricted use, distribution, and reproduction in any medium, provided the original author and source are credited.

ABSTRACT

In this study, cerium oxide nanoparticles (CeO₂ NPs) were synthesized using a green chemistry approach, utilizing quince fruit (Cydonia oblonga) peel extract as a non-toxic reducing and stabilizing agent. This environmentally friendly technique represents a novel approach to nanoparticle fabrication, emphasizing sustainability in nanotechnology. The surface of the green-synthesized CeO2 NPs was further functionalized with cidofovir (CDV), an anti-DNA virus agent, to develop a dualfunctional therapeutic platform with potential anticancer and antiviral applications. The successful synthesis and modification of CDV-loaded CeO₂ NPs (CDV- CeO₂ NPs) were confirmed through a series of characterizations, including FT-IR, zeta potential, TEM, SEM-EDX, DLS, and UV-Vis analyses. The cytotoxic effects of CDV, CeO₂ NPs, and CDV- CeO₂ NPs were evaluated against the MCF-7 breast cancer cell line using the MTT assay, revealing that the loading of CDV onto CeO₂ NPs significantly enhanced its anticancer efficacy. Furthermore, the interaction of CDV-CeO2 NPs with nucleic acids (DNA and RNA) was investigated through absorption and fluorescence studies, demonstrating a strong binding affinity and suggesting the potential of these nanoparticles as highly specific chemotherapeutic agents. The novelty of this work lies in the innovative green synthesis method, the dual-functional therapeutic application, and the enhanced biological activity of the CDV-CeO2 NPs, which collectively position these nanoparticles as promising candidates for future cancer and antiviral therapies.

INTRODUCTION

In recent years, metal oxide nanoparticles (MO-NPs) have attracted increasing attention due to their exceptional properties and wide-ranging applications. The production of MO-NPs has become a focal point in nanotechnology, as their demand continues to grow in various industries and medical fields, such as fillers, sterilizers, optical devices, catalytic products, drug delivery and antimicrobial agents [1]. Cerium, a rare earth element, exhibits unique chemical behavior that distinguishes it from transition elements, alkaline earth

and post transition. This behavior can be attributed to the shielding effect and the characteristics of its 4f orbitals, which endow rare earth elements with specific catalytic, magnetic, photocatalytic, and electronic properties [2, 3]. These distinctive features enable innovative applications that cannot be achieved with transition elements. CeO₂ NPs, or nanoceria, primarily exhibit two self-regenerating oxidation states: Ce⁴⁺ and Ce³⁺. Nanoceria possesses a range of remarkable properties, including such as nonstoichiometric, reduction behavior, oxygen storage capacity, large magnetic moment, high complexation property, and high conductivity. Furthermore, small-scale

¹Inorganic Chemistry Department, Faculty of Chemistry, Razi University, Kermanshah, Iran

²Medical Biology Research Center, Health Technology Institute, Kermanshah University of Medical Sciences, Kermanshah, Iran

ceria can exhibit unique characteristics, such as a larger band gap compared to its bulk counterpart [4]. Nanoceria has shown promise as an effective treatment for neurodegenerative diseases and holds numerous potential applications as antioxidants in biological systems, catalysts, and in fuel cells. Moreover, other biological properties of nanoceria have been reported, such as antiinflammatory, antitumor [5], and enzyme mimetic activities including scavenging hydroxyl radicals, superoxide dismutase (SOD), peroxidase and catalase have also been reported [6, 7]. Nanoceria has been the focus of many in vivo and in vitro researches, especially in the field of tumor microenvironments (TME) as a cytotoxic agent [8]. Its oxidative stress-induced properties have been found to increase tumor cell membrane leakage without harming healthy cells, which can aid in the design of new drugs [9, 10]. Moreover, nanoceria has been employed to protect primary cells from radiation therapy's adverse effects and serve as potential drug delivery platforms [11]. The scientific literature highlights the significance of nanoceria in the development of novel therapeutic drugs [12–16]. Various synthesis methods for nanoceria have been developed, such as sol-gel [17], hydrothermal [18], precipitation [19], solvothermal [20], emulsion technique [21], combustion synthesis [22], microwave approach [23], and thermal decomposition [24]. However, chemical methods involve toxic chemicals, capping agents or additives, and non-polar solvents, making them unsuitable for biomedical applications. As a result, many researchers are searching for biocompatible and eco-friendly methods to synthesize nanoparticles and are exploring biosynthesis techniques. In nanotechnology, the biosynthesis process plays a critical role as it eliminates harmful byproducts from specific chemical reactions and enables a solvent-free organic synthesis protocol. Additionally, it is easily scalable for large-scale production and is cost-effective. The extracts of plant, egg white, honey, and fungal extracellular compounds, have been employed as both reducing and capping agents in synthesis of nanoparticle [15, 25, 26]. These biocomponents contribute to the production of nanocrystalline metal oxide nanoparticles with varying morphologies and sizes. The Quince Fruit (Cydonia oblonga) is a member of the Rosaceae family and is known by various names such as "Bahee Dana" in Urdu, "Beh" in Farsi, "Strythion" in Greek, and "Bihi" in Hindi. It is indigenous to western Asia, stretching from Iran to Turkestan, and has been used since ancient times, with its origin dating back to Persia around 4000 BC. The fruit has spread throughout the Mediterranean basin to the west and Afghanistan to the east, along with the flourishing civilizations of that era [27, 28]. Nowadays, quince is cultivated in various regions worldwide, including many European nations, Oceania, South America, Australia, and North and South Africa [29], the Mediterranean, and parts of Asia. It grows wildly in different regions of Iran, such as Azerbaijan, Gilan and Golestan. Quince fruit is composed of vitamins B1, B2, PP, and C, organic acids (malic acid, citric acid), carbohydrates (starch, fructose, glucose), carotene, tannins, aromatic compounds, fiber magnesium, phosphorus, potassium salts, calcium, proteins. Notably, it contains well-known antioxidants like caffeoylquinic acids and rutin, with the peel being a rich source of caffeoylquinic acid, along with other significant flavonoids such as quercetin 3-galactoside, kaempferol-3-rutinoside and kaempferol 3-glucoside [30]. These compounds contribute to the formation of nanosistines and alter their surface. The fruit's most beneficial components are the polyphenols with antioxidant potential, found in its peel, leaves, and seeds [31–34]. The current approach to inhibit cancer cell growth using anticancer drugs like doxorubicin, paclitaxel, and cisplatin is associated with undesirable side effects such as fever, vomiting, mouth sores, and hair loss. Developing effective anticancer drugs with fewer side effects is a time-consuming process. However, drug efficacy can be improved, side effects can be reduced, or drugs can be delivered in a targeted manner to expedite the process [35]. Antiviral drugs are a specific class of medications used to treat viral infections [36]. CDV (see Figure 1), also known as (S)-1-(3-hydroxy-2-

Figure 1: The molecular structure of antiviral drug cidofovir (CDV).

(phosphonomethoxy) propyl) cytosine dihydrate (HPMPC), is an antiviral medication that belongs to a novel family of drugs. Cervical cancer and a significant proportion of head and neck squamous cell carcinomas (HNSCC) are caused by the human papillomavirus (HPV). Cidofovir has been found to be effective in treating various HPV-induced benign and malignant hyperproliferation. Mertens et al. reported that the antiproliferative effects of CDV are due to its incorporation into DNA, which leads to DNA damage [37]. Hadaczek and colleagues reported that CDV exhibits potent antineoplastic activity against HCMV-infected glioblastoma cells by inhibiting HCMV gene expression and inducing cellular apoptosis [38]. They also found that CDV induces glioblastoma cell death in the absence of HCMV infection by integrating into tumor cell DNA and promoting double-stranded DNA breaks, leading to apoptosis. When combined with ionizing radiotherapy, the standard treatment for glioblastoma in humans, CDV enhances radiation-induced DNA damage and further induces tumor cell death. The combination of CDV and radiotherapy significantly prolonged the survival of mice with intracranial glioblastoma tumors. Investigating the interactions between small molecules and nucleic acids has been a significant area of research for many years [39, 40], RNA and DNA are important pharmacological targets for many antibiotics and anticancer drugs. Comprehensive knowledge of the molecular mechanisms underlying the interaction between small ligands and nucleic acids is essential for the development of potent RNA-binding

antiviral compounds and DNA- or RNA-based anticancer drugs. This study presents the first-ever production of CDV-loaded green synthesized cerium oxide nanoparticles (CDV-CeO₂ NPs) derived from quince fruit peel extract and their characterization studies. We have investigated the structural and anticancer properties and the interactions between DNA/RNA and CDV-CeO₂ NPs. This study is the first of its kind on the green synthesis of CDV-CeO₂ NPs employing quince peel extract and their nucleic acid interaction investigations. Although some nanocarriers have been developed and utilized for targeted anticancer drug delivery, their effects on processes such as DNA and RNA interactions are not fully understood. Therefore, this study aimed to explore the DNA and RNA interactions of CDV-CeO₂ NPs and demonstrate the impact of CDV-CeO₂ NPs on binding mode employing physico-chemical techniques.

RESULTS AND DISCUSSION

The characterization of CeO₂ NPs synthesized through a green process

Electronic absorption titration

Figure 2 depicts the UV-Visible spectra of green synthesized CeO₂ NPs, CDV, and CDV-CeO₂ NPs. The absorption peaks are between 250 to 400 nm for green synthesized CeO₂ NPs which, is due to the charge

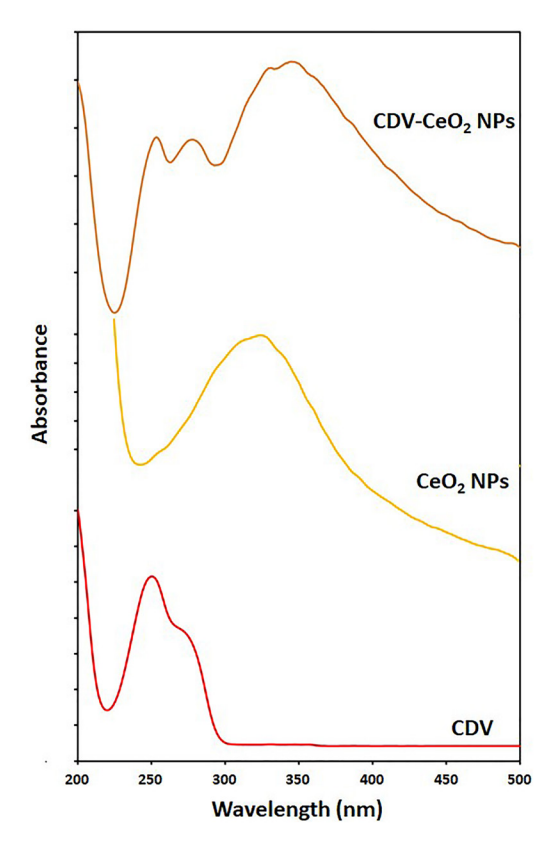


Figure 2: UV-vis spectra of CDV, CeO₂ NPs and CDV-CeO₂ NPs.

transfer from O_{2P} to Ce_{4f} orbitals [41]. As can be seen, the absorption peak between 250 to 400 nm for CDV-CeO₂ NPs shifted toward long wavelength about 21 nm, which authenticated that the loading of drug had successfully happened. Moreover, the bands at 253 nm and 278 nm were developed (similar to the maximum wavelength of the drug), which proved the presence of surface loaded on the structure of the CeO₂ NPs [42].

To determine the drug loading amount on the CeO₂ NPs that were synthesized using green methods, an ultraviolet-visible spectrophotometer was used. The supernatant, collected through centrifugation, was used to measure the amount of unloaded drug at 249 nm. The efficiency of the drug loading was then determined using the standard curve equation.

$$y = 34.288x + 0.1379 \tag{1}$$

The efficiency of CDV loading was estimated about 30%.

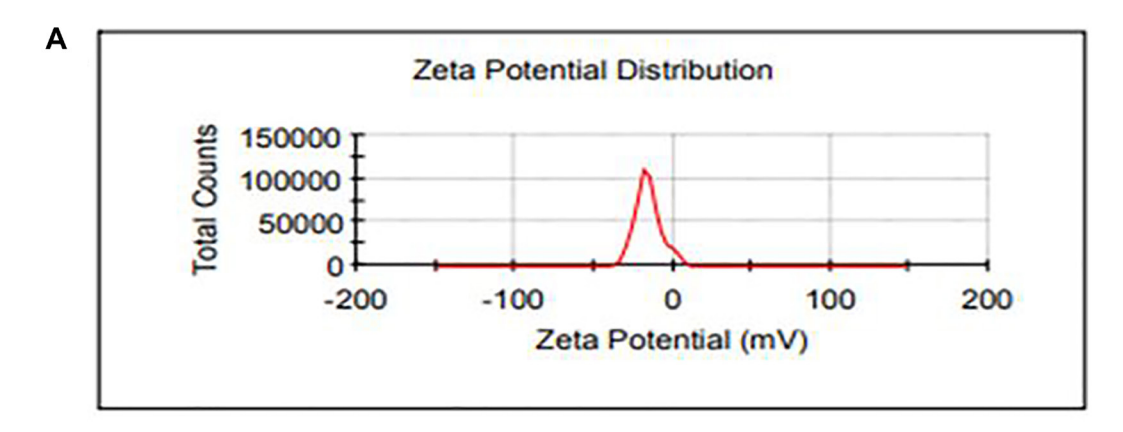
Zeta Potential and DLS measurements of CeO₂ NPs

DLS was utilized to measure the size distribution of CeO₂ NPs and CDV-CeO₂ NPs. Zeta sizer was also employed to identify the surface charge on CeO₂ NPs and CDV-CeO₂ NPs. Figure 3 represents the negative surface charge value (-15.6 and -33.5 mV) on the CeO₂

NPs and CDV-CeO₂ NPs, respectively, which indicates the negative-negative repulsion that leads to their high degree of stability [43]. Monodispersity of CeO₂ NPs and CDV-CeO₂ NPs were also reflected by the sharpness of the DLS peaks [44]. As revealed in Figure 4 the average size of CeO₂ NPs and CDV-CeO₂ NPs is 128.4 and 261.2 nm, respectively. It is clear that the CDV-CeO₂ NPs' average size increased, confirms the presence of a layer of CDV on the CeO₂ NPs [45].

FE-SEM and EDX analysis

FE-SEM technique was utilized to analyze the morphology of CeO₂ NPs and CDV-CeO₂ NPs. FE-SEM images demonstrated agglomeration of CeO₂ NPs. The CeO₂ nanoparticles exhibit a flake-like structure (see Figure 5A) [46]. As can be seen, the CDV loading on the CeO₂ NPs structure leads to an alteration in the CeO₂ NPs' morphology (see Figure 5B). It is obvious that the small granules or grains confirm the presence of the drug on CeO₂ NPs [47]. The compositional analysis of CeO₂ NPs and CDV-CeO₂ NPs were illustrated by utilizing EDX analysis (see Figure 6). EDX analysis results of CeO₂ NPs revealed high intensity peaks of Ce and O, as well as C, N, and Cl, which is from plant extract [46]. As shown in EDX results of CDV-CeO₂ NPs, the strong band of P confirms the presence of surface loaded CDV on the structure of the green synthesized CeO₂ NPs [48].



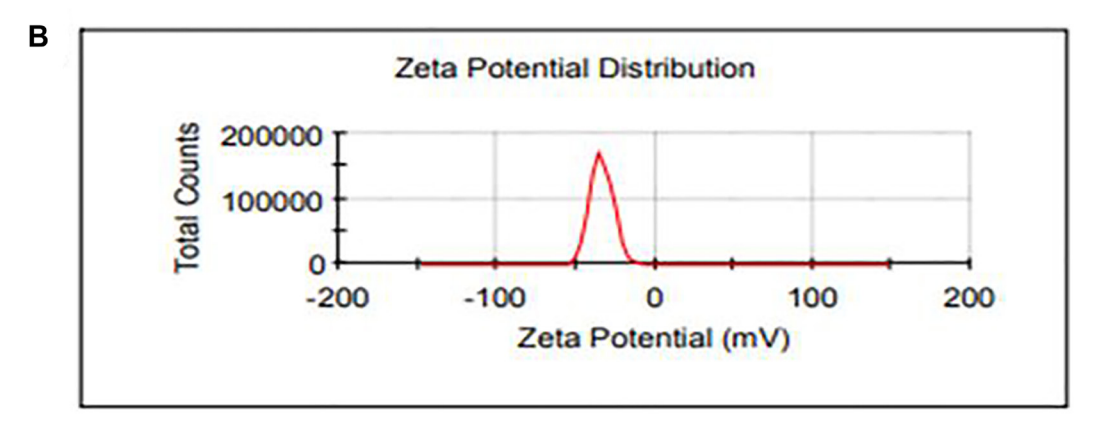


Figure 3: Zeta potential distribution of (A) CeO₂ NPs and (B) CDV-CeO₂ NPs.

TEM images

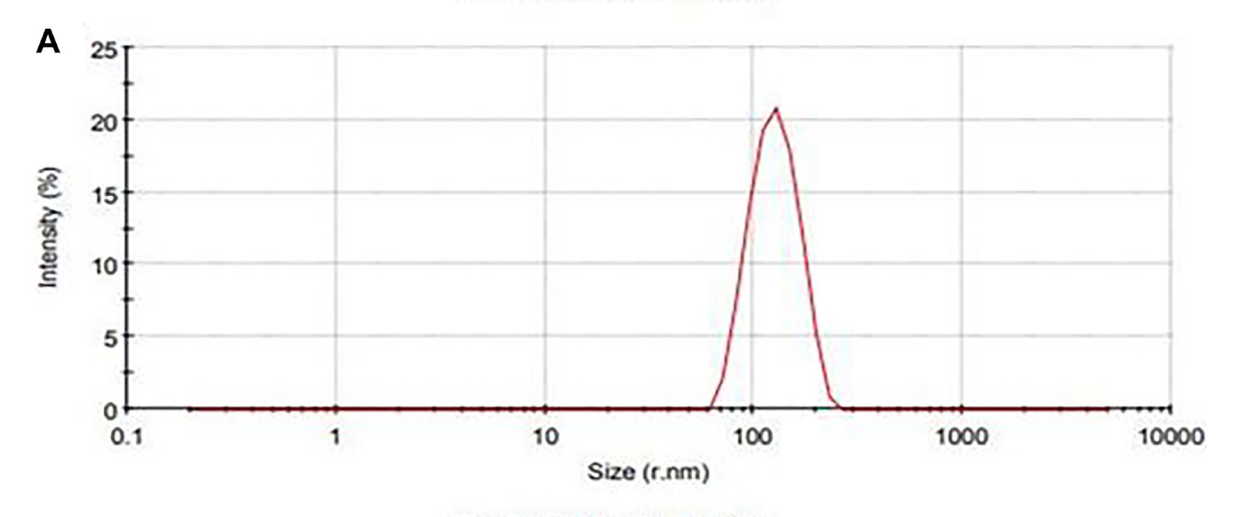
To detect the shape and size of the green-synthesized CeO₂ nanoparticles, TEM technique was employed. The core-shell structure of the nanoparticles can be observed in Figure 7, where CeO₂ NPs constitute the inner sphere, and the drug forms the outer shell. The TEM images revealed that the agglomerated NPs had a diameter size of 156.96 nm, while single NPs had a diameter of 14.90 nm. The CeO₂ NPs agglomeration was observed to be high in aqueous media due to their high surface energy. In the image, the CeO₂ NPs are depicted as the dark area within the core, whereas the drug is shown as a silver-gray outer shell.

Functional group analysis

Fourier transform infrared spectroscopy was used to identify the functional groups present in CDV, CeO₂ NPs, and CDV-CeO₂ NPs in the range of 500–4000 cm⁻¹, and

the results were tabulated in Figure 8. The broad absorption band observed at 3750-3000 cm⁻¹ is due to the Ce-OH and O-H stretching from residual alcohols and water [49]. Our green synthesized CeO₂ NPs showed absorption bands at 3550, 3474, and 3414 cm⁻¹. Minor distortions in the 2030 cm⁻¹ range indicate the presence of NH bonds in the Cydonia oblonga peel extract in the resulting CeO₂ NPs [50]. The peaks observed at 1384 and 1616 cm⁻¹ may be due to the C-H and C=O stretching vibrations of residual organic compounds, respectively [41]. The peak observed at 1116 cm⁻¹ can be attributed to the overtone band of the trace of Ce-OH [51]. The bands at 482, 621, and 856 cm⁻¹ can be correlated with the stretching frequency of Ce-O and the formation of CeO₂ [52]. The FT-IR spectra of CDV show specific wavenumbers, namely 1715, 1634, 1486, 1011, and 1107 cm⁻¹. The absorption peaks at 1107 and 1011 cm⁻¹ correspond to the stretching vibration of P=O and P-O bonds, respectively. Additionally, the FT-IR spectra show the OH group of the cidofovir structure at 3313 cm⁻¹ [53]. The FT-IR spectrum of CDV-CeO₂ NPs

Size Distribution by Intensity



Size Distribution by Intensity

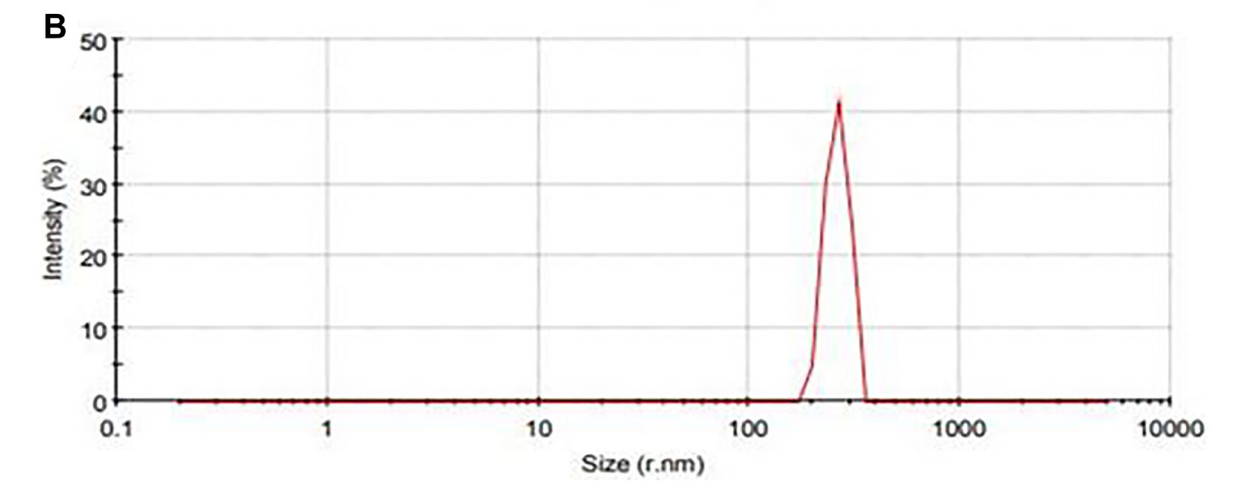


Figure 4: DLS particle size analysis of (A) CeO₂ NPs and (B) CDV-CeO₂ NPs.

demonstrates the characteristic peaks of CeO₂ NPs and CDV, which is consistent with the formation of the CDV-CeO₂ NPs structure [48].

Cytotoxic assess

Figure 9 illustrates the inhibitory potential and sensitivity of CDV, CeO₂ nanoparticles, and CDV-CeO₂ nanoparticles against cancer cell growth at different concentrations. The anticancer activity increased with increasing treatment concentrations. At the highest

concentration (64 μg/mL), the mortality rate of MCF-7 cancer cells was 71.65% for CDV, 49.85% for CeO₂ nanoparticles, and 97.10% for CDV-CeO₂ nanoparticles. The IC₅₀ values were found to be 21.83 μg/mL, 40.11 μg/mL, and 4.46 μg/mL for CDV, CeO₂ NPs, and CDV-CeO₂ NPs, respectively. The results indicate that CDV-loaded CeO₂ NPs exhibit more pronounced anticancer activity than CDV and CeO₂ NPs alone. This suggests that loading CDV on CeO₂ NPs leads to a significant enhancement of the anticancer and biological effects of CDV [54].

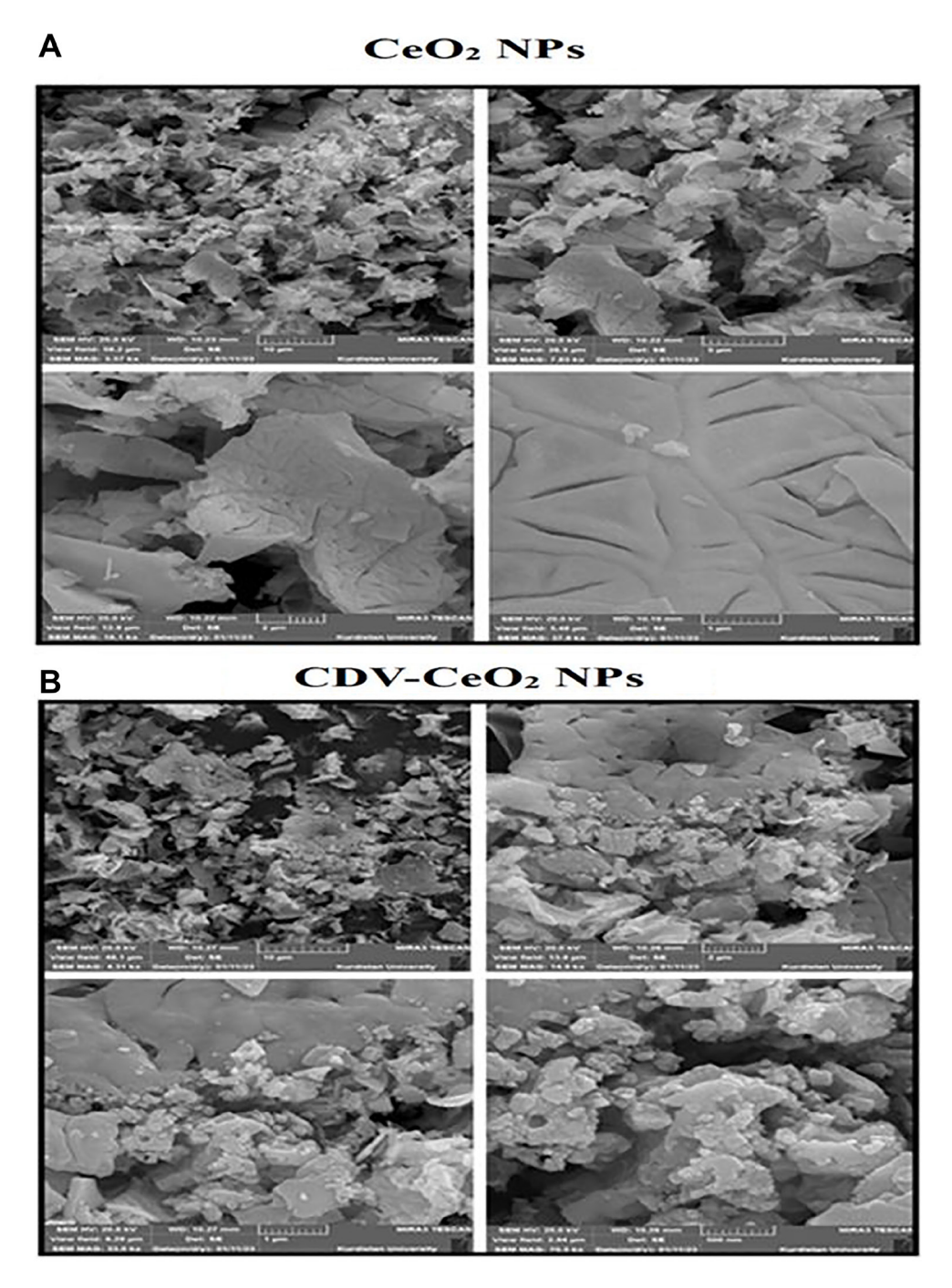


Figure 5: SEM images of (A) CeO₂ NPs and (B) CDV-CeO₂ NPs.

The results of this study are also comparable with the work conducted by Karampour et al. [55], in which magnetic $\gamma\text{-Fe}_2O_3@SiO_2$ NPs loaded with CDV were synthesized and their cytotoxicity against MCF-7 cells was evaluated. At the highest tested concentration (160 µg/mL), the cell mortality rate for $\gamma\text{-Fe}_2O_3@SiO_2\text{-CDV NPs}$ was reported to be 75.84%, and the IC50 value was 74.26 µg/mL. In comparison, the CDV-CeO2 NPs synthesized in the present study exhibited significantly stronger anticancer effects at a lower concentration, with an IC50 value of only $4.46 \pm 0.22~\mu\text{g/mL}$ approximately 17 times lower.

According to the obtained results, this compound can be considered a novel and effective candidate for the design of targeted drug delivery systems in breast cancer chemotherapy. However, to confirm the efficacy and safety of this nanocarrier for clinical applications, further studies including *in vivo* experiments, pharmacokinetic assessments, and detailed investigations of the underlying molecular mechanisms are necessary.

Ct-DNA and RNA interaction

UV-vis spectroscopy

To assess the formation of CDV-CeO₂ NPs-DNA and CDV-CeO₂ NPs-RNA complexes, the ultraviolet-

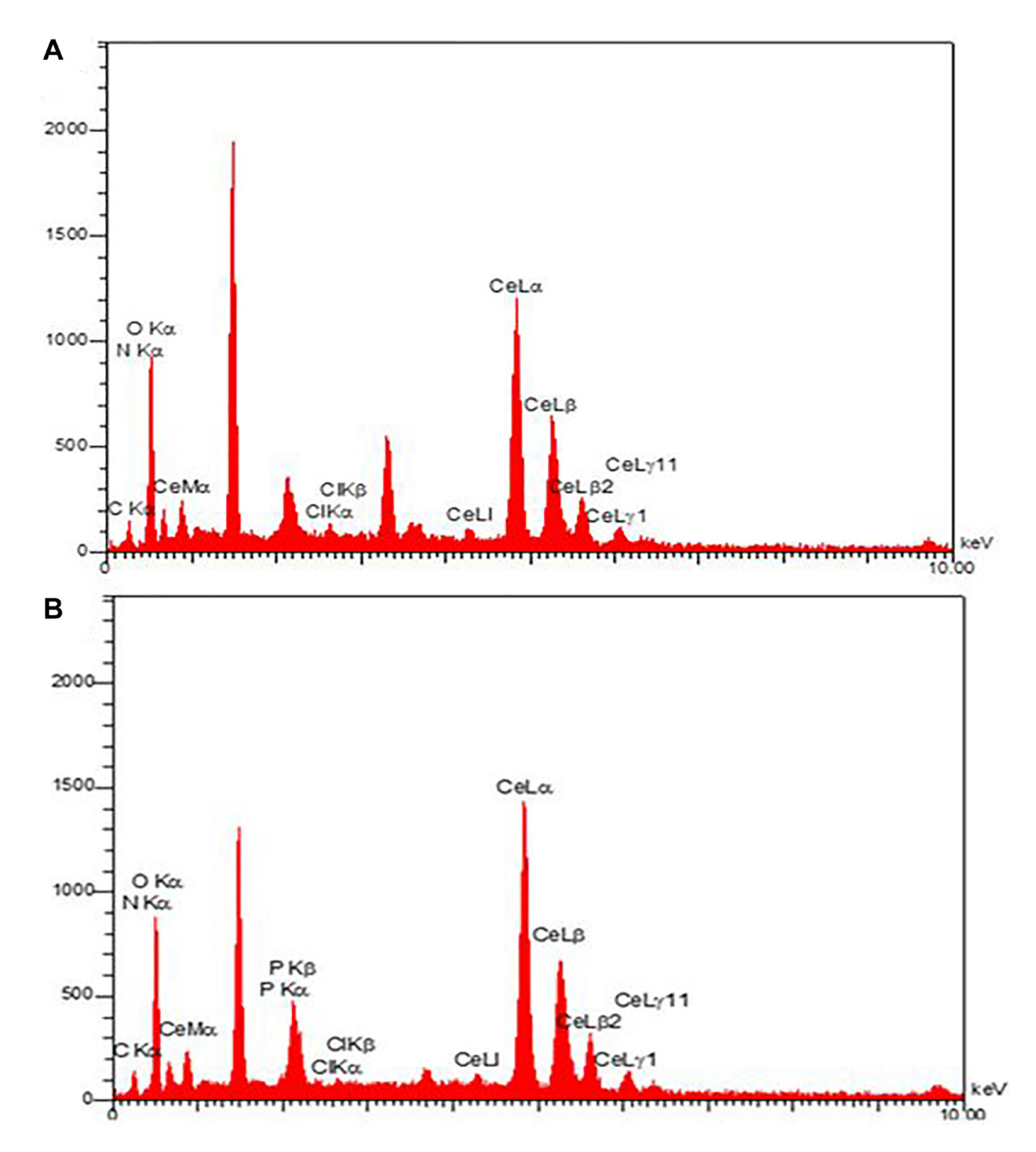


Figure 6: EDX images of (A) CeO₂ NPs and (B) CDV-CeO₂ NPs.

visible absorption spectra of DNA/RNA with and without CDV-CeO₂ NPs were examined. Figures 10A and 11A indicate that the DNA/RNA absorption spectra exhibited hypochromism, which resulted from the formation of a ground-state complex with CDV-CeO₂ NPs. Furthermore, the isosbestic point indicated the formation of a new CDV-CeO₂ NPs-nucleic acid complex, demonstrating that the binding of CDV-CeO₂ NPs to DNA and RNA indeed occurred [56].

The Wolfe–Shimmer equation was used to calculate the association constant of the nucleic acids and CDV-CeO₂ NPs interaction:

$$1/(A - A_0) = 1/(A - A_0) + 1/K_b(A_{\infty} - A_0).1/(CDV - CeO_2 NPs)$$
(2)

Where, A_0 is the free nucleic acids 'absorbance at 260 nm, and A is the absorbance of biomolecule with

CDV-CeO $_2$ NPs. To calculate the binding constant (K_b) of biomolecule-CDV-CeO $_2$ NPs system the plot of 1/(A-A $_0$) versus 1/(CDV-CeO $_2$ NPs) was employed (see Figures 10B and 11B). The obtained K_b value was 3.63 × 10 3 and 1.26 × 10 3 M (M = g/mL) for DNA and RNA, respectively. The spectrofluorimetry technique can give a mechanistic detail of the exact nucleic acids - CDV-CeO $_2$ NPs system' binding mode. Thus, it was used to explore the mode of binding in this study.

Fluorescence studies

Fluorescence method was employed to further assess the interactions of nucleic acids with CDV-CeO₂ NPs. DNA and RNA alone exhibit a weak fluorescence signal because of their fluoresce quenching by solvent molecules. Also, in aqueous solution, AO and HO exhibit

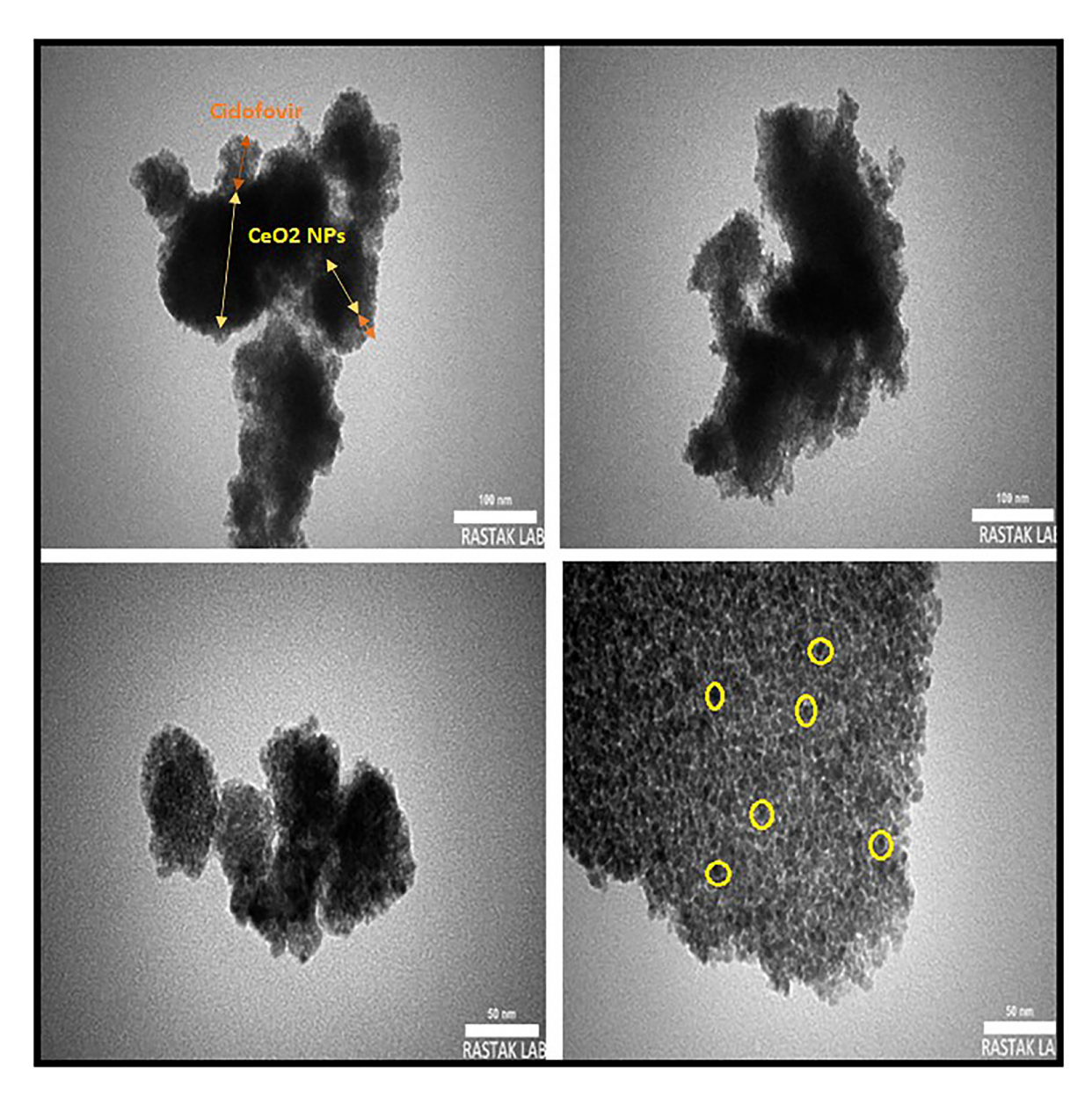


Figure 7: TEM images of CDV-CeO₂ NPs with different magnification.

low fluorescence in their free state but show an increase in emission intensity upon interaction with DNA/RNA. The emission intensity of RNA-AO and RNA-HO system was recorded on subsequent addition in enhancing amounts of CDV-CeO₂ NPs. The RNA-AO system' emission intensity decreased upon elevating the CDV-CeO2 NPs different concentrations (see Figure 12). This result indicated that CDV-CeO₂ NPs block the site for bonding of AO, that is, they have the same binding region on RNA. As can be seen, RNA represents a weak interaction with HO and the there is a negligible enhancement in the fluorescence intensity of HO in the presence of RNA (see Figure 13). This is believed to be due to the shallow minor grooves of RNA. Additionally, the addition of CDV-CeO₂ NPs to the HO-RNA solution did not result in any significant changes in fluorescence intensity. Therefore, we conducted fluorescence measurements at three different temperatures (288.15, 298.15, 310.15 K) by using AO to determine the binding constant.

The emission intensity of DNA-AO and DNA-HO system was recorded on subsequent addition in enhancing amounts of CDV-CeO₂ NPs. As Figures 14 and 15 show, the emission intensity of the systems (DNA-AO and DNA-HO) is strongly affected by different concentrations of CDV-CeO₂ NPs. The DNA-AO system' emission intensity decreased upon elevating the CDV-CeO2 NPs ' different concentrations. This result indicated that CDV-CeO₂ NPs intercalated to DNA helix, thereby block the site for bonding of AO. Besides, with addition, of various amounts of CDV-CeO₂ NPs the DNA-HO 'emission intensity decreased, showing that CDV-CeO₂ NPs remove HO from the DNA grooves. So, analysis of the data show that CDV-CeO₂ NPs interact with DNA both through the groove and intercalate (partial intercalation) [57]. Therefore, we conducted fluorescence measurements in the presence of both AO and HO at three distinct temperatures (288.15, 298.15, and 310.15 K) to calculate the binding constant.

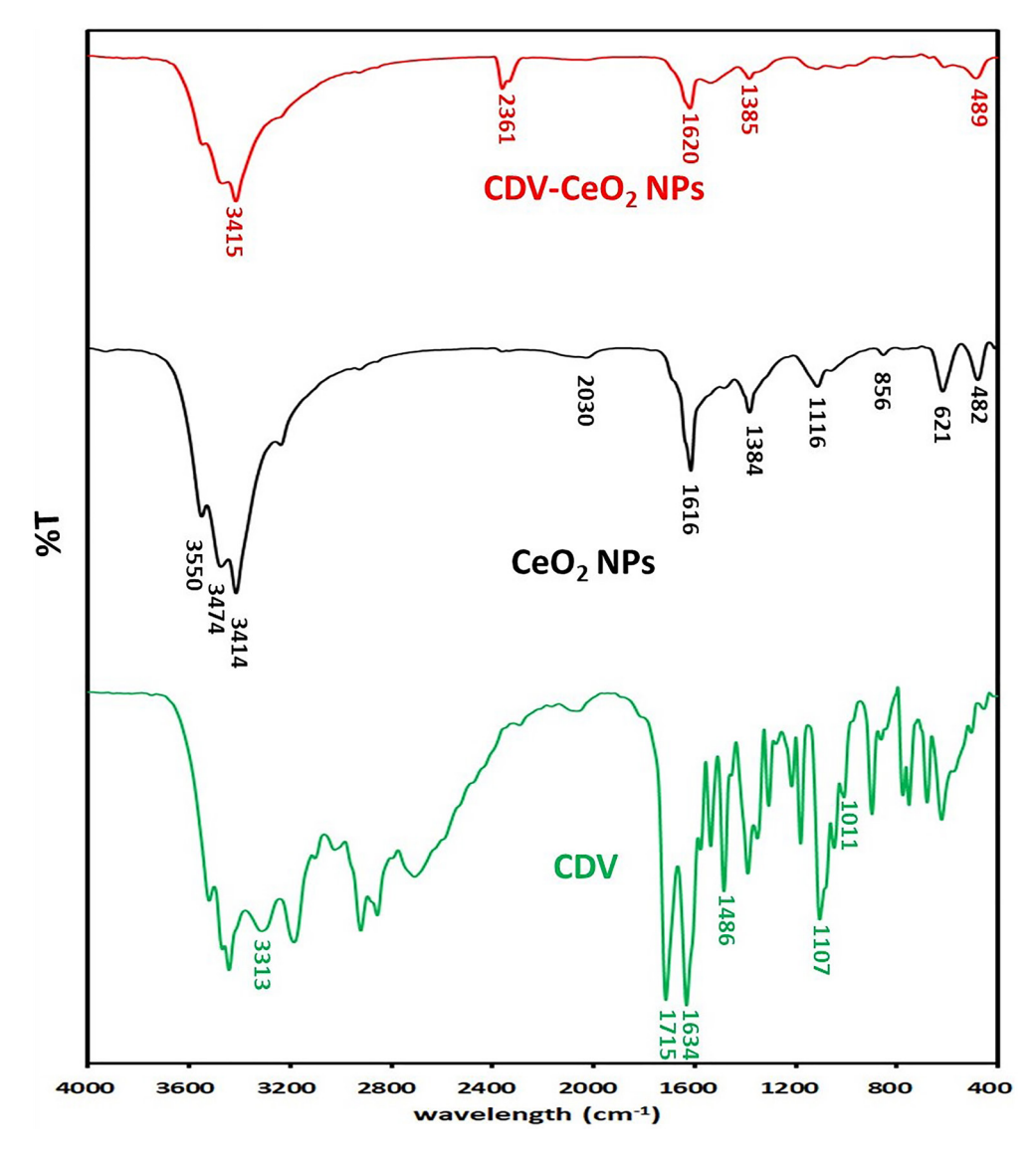


Figure 8: FTIR spectra of CDV, CeO₂ NPs and CDV-CeO₂ NPs.

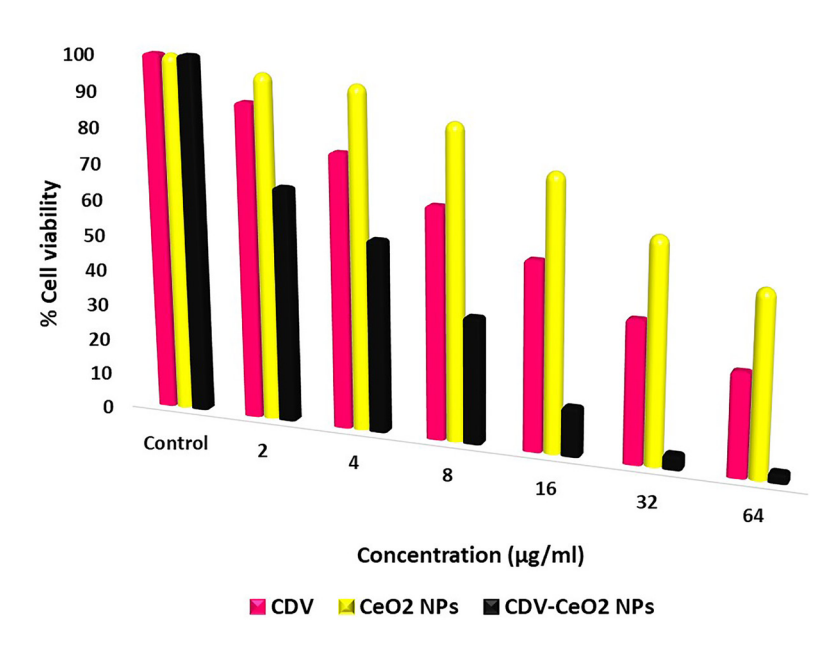


Figure 9: CDV, CeO₂ NPs and CDV-CeO₂ NPs on cell viability.

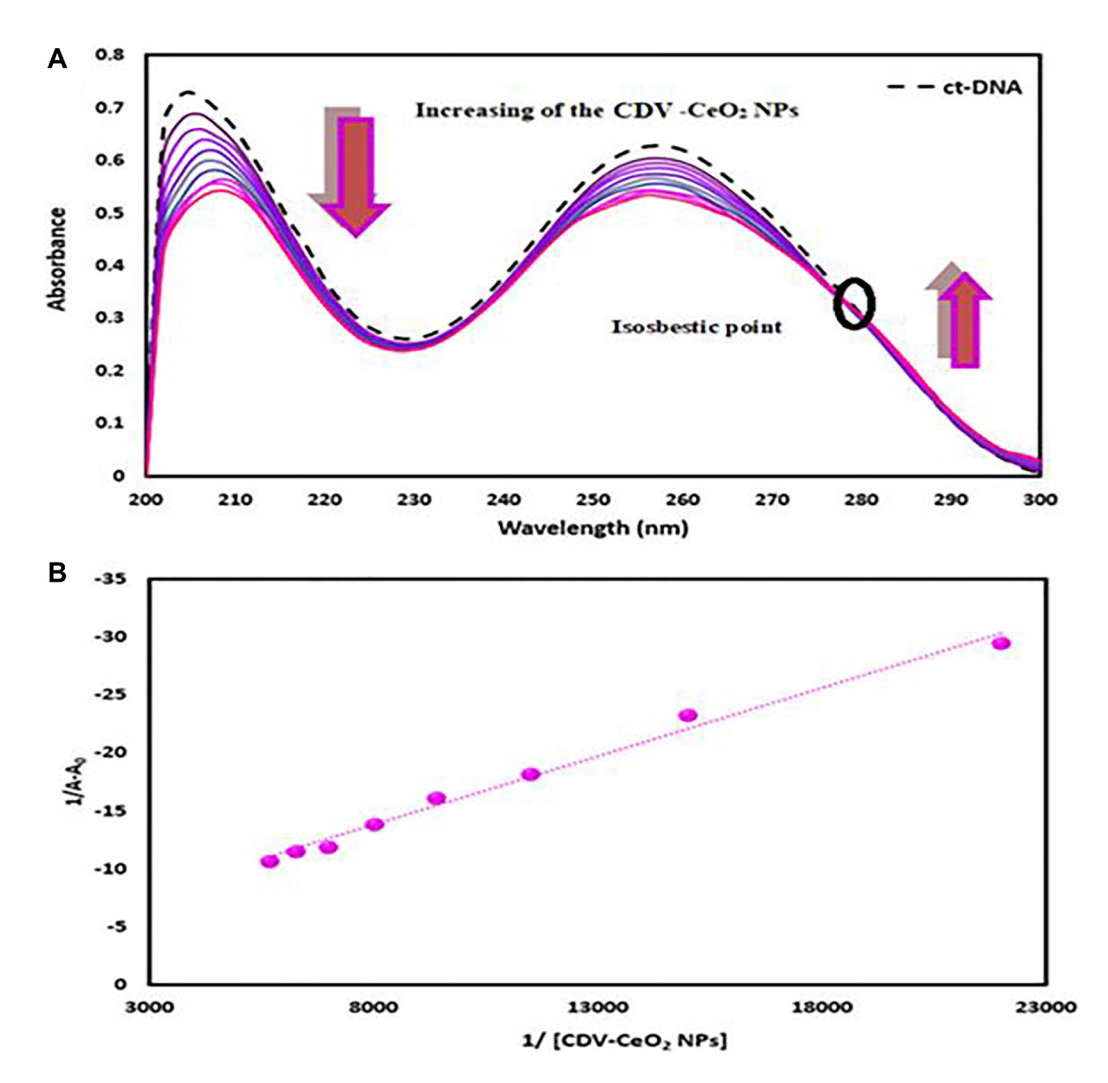


Figure 10: (A) Absorbance spectra of ct-DNA $(4.00 \times 10^{-5} \text{ M})$ with green synthesized CDV-CeO2 NPs $(2.32 \times 10^{-5} \text{ to } 1.76 \times 10^{-4} \text{ g/mL})$. (B) Wolfe-shimmer plot of ct-DNA- CDV-CeO2 NPs.

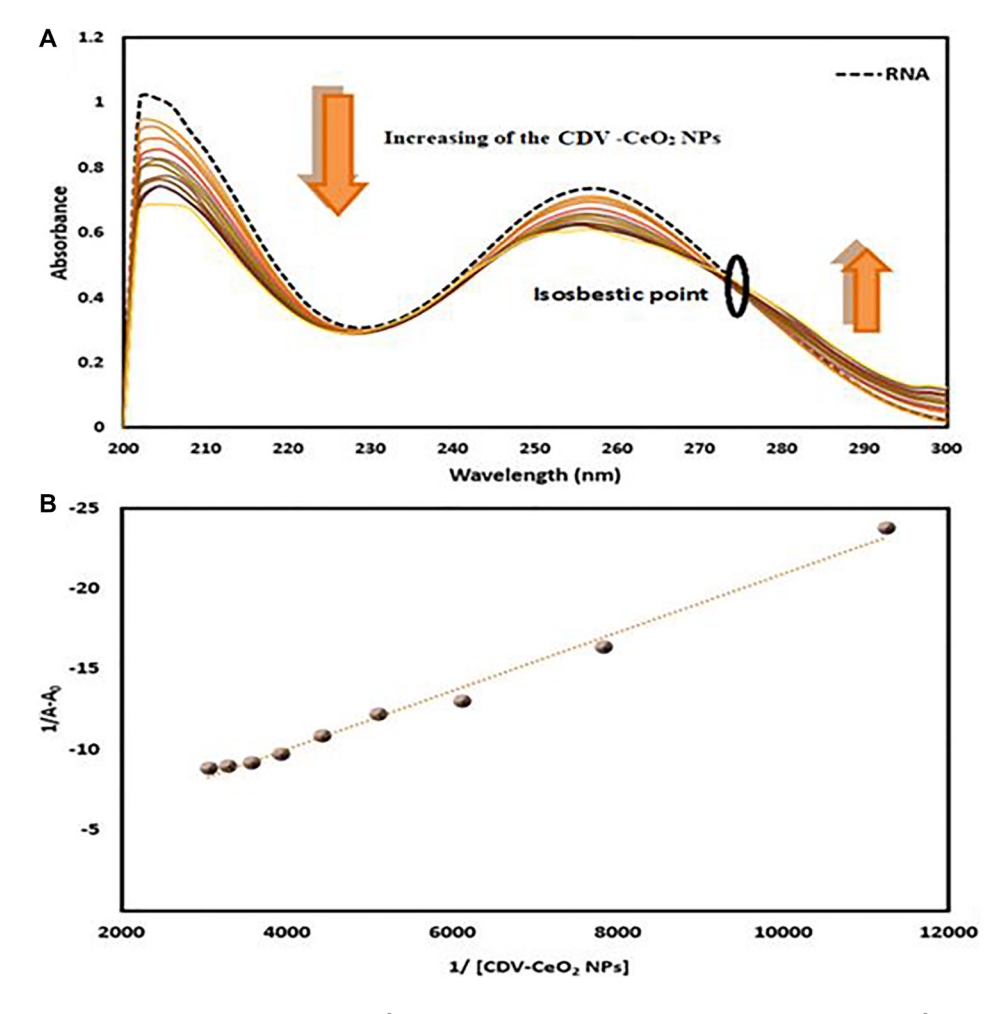


Figure 11: (A) Absorbance spectra of RNA $(4.00 \times 10^{-5} \text{ M})$ with green synthesized CDV-CeO₂ NPs $(2.32 \times 10^{-5} \text{ to } 1.76 \times 10^{-4} \text{ g/mL})$. (B) Wolfe-shimmer plot of RNA- CDV-CeO₂ NPs.

Increasing of the CDV-CeO₂ NPs

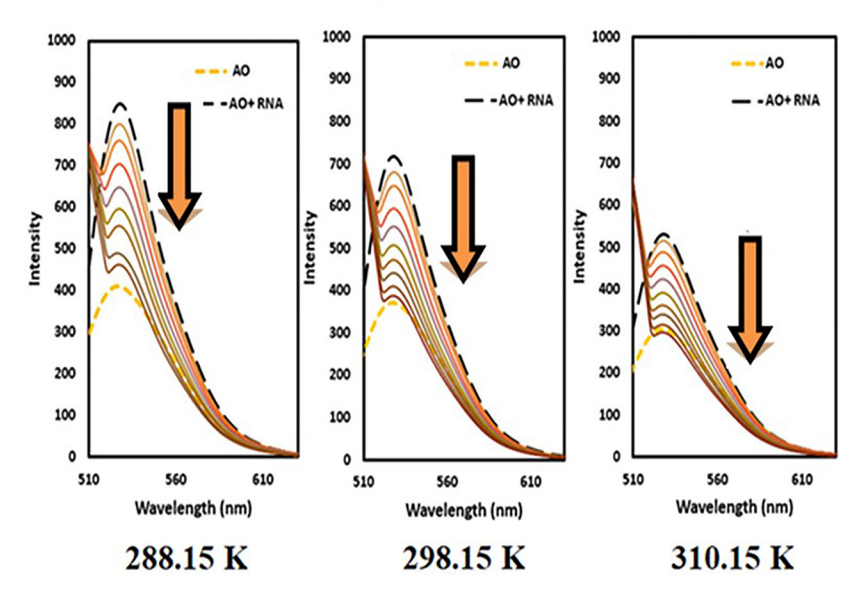


Figure 12: Fluorescence spectra of AO + RNA in the presence of CDV-CeO₂ NPs (2.44 × 10⁻⁵ to 2.59 × 10⁻⁴ g/mL), RNA = $(1.76 \times 10^{-4} \, \text{M})$ C_{AO} = $(5.00 \times 10^{-6} \, \text{M})$.

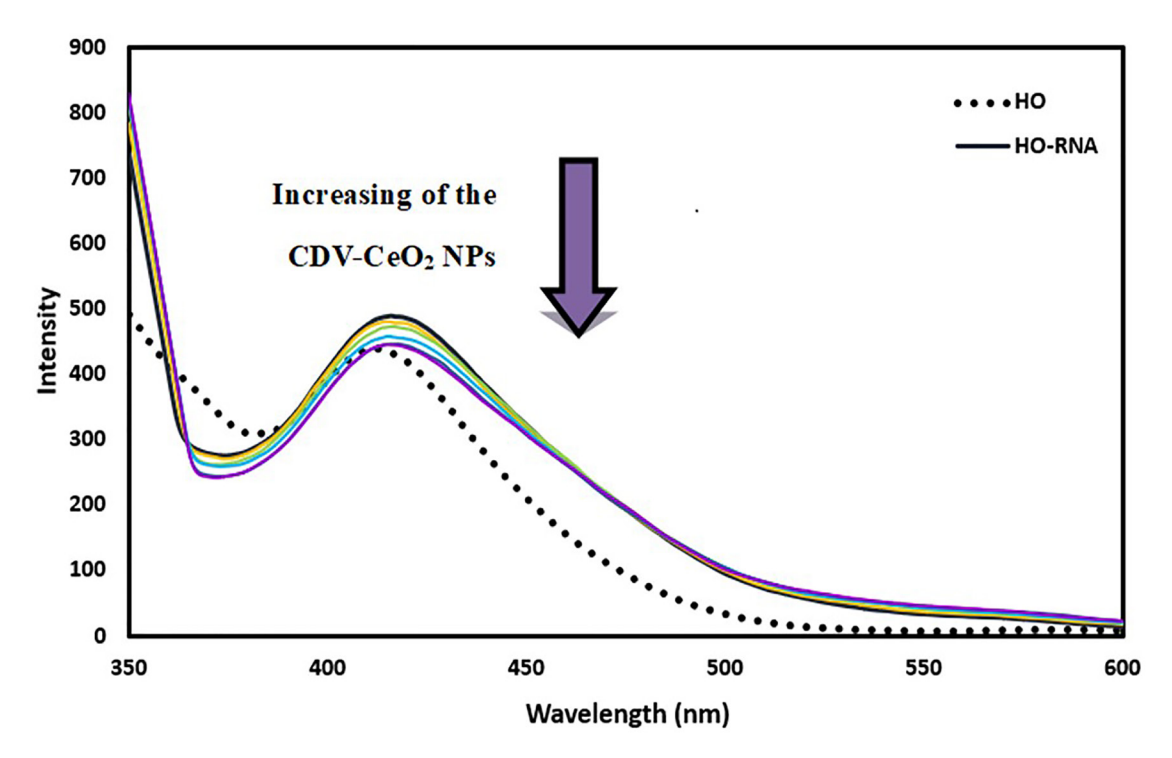


Figure 13: Fluorescence spectra of Hoechst + RNA in the presence of CDV-CeO₂ NPs (2.44 \times 10⁻⁵ to 2.59 \times 10⁻⁴ g/mL), RNA = (1.76 \times 10⁻⁴ M) C_{Hoechst} = (5.00 \times 10⁻⁶ M).

Increasing of the CDV-CeO₂ NPs

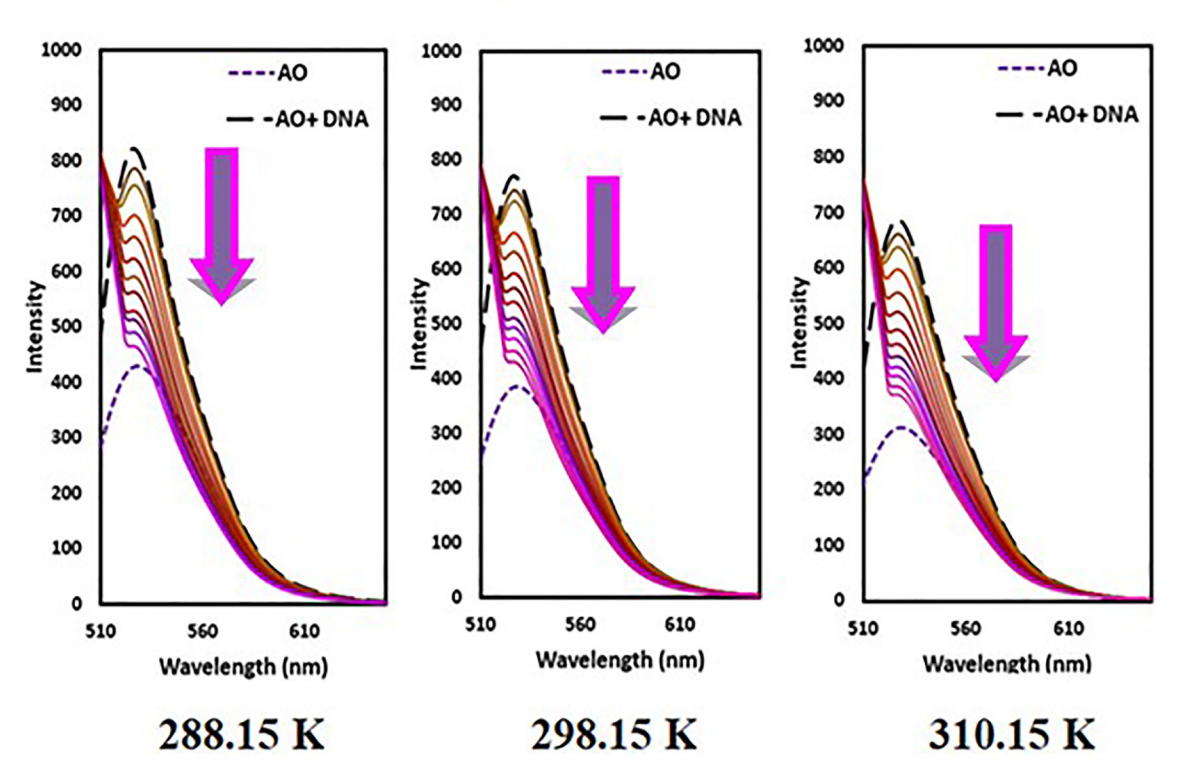


Figure 14: Fluorescence spectra of AO + DNA in the presence of CDV-CeO₂ NPs (2.44 × 10⁻⁵ to 2.59 × 10⁻⁴ g/mL), DNA = $(1.76 \times 10^{-4} \,\mathrm{M})$ C_{AO} = $(5.00 \times 10^{-6} \,\mathrm{M})$.

To determine whether the quenching mechanism of the CDV-CeO₂ NPs/labeled nucleic acids system is static or dynamic in nature, we utilized the following Stern-Volmer equation (Eq. 3) [58]:

$$F_0/F = 1 + K_{sv}(Q) = 1 + \tau_o kq$$
 (3)

The emission intensity of labeled nucleic acids in the absence and presence of CDV-CeO2 NPs is represented by F_0 and F, respectively. τ_0 is the labeled nucleic acids' lifetime in the absence of CDV-CeO₂ NPs, (Q) is the concentration of CDV-CeO₂ NPs, Ksv is the Stern-Volmer quenching constant, and kq is the apparent bimolecular quenching rate constant, which is calculated based on Ksv = kq τ_o [59]. The Stern-Volmer quenching constant was obtained from the slope of the plot of F₀/F vs. (CDV-CeO₂ NPs) (see Figures 16A, 17A and 18A). Since the interaction of RNA with the CDV-CeO₂ NPs in the presence of HO was not satisfactory, we calculated the binding constant for the RNA + AO system with increased CDV-CeO2 NPs. For RNA the values of K_{sv} showed decreased with the temperature rise (see Table 1), revealed that static quenching was the primary process involved in the complex formation [60]. For DNA-AO and DNA-HO systems, the $K_{\mbox{\tiny sv}}$ values increased on rising the temperature (see Tables 2 and 3), which implied that dynamic quenching is the main process involved in the complex formation. Dynamic quenching only impacts the excited state of the quenching molecule and does not alter the absorption spectrum of DNA. On the other hand, in static quenching, a complex of DNA and ligand is formed, resulting in alterations in the UV-visible spectra of DNA. The results of the UV-Vis experiment (see Figure 10A) further confirmed that static quenching is the primary quenching mechanism for the DNA-CDV-CeO2 NPs complex [61].

Determination of the binding constant (K_b) and number of binding sites (n) can be done using the following equation:

$$Log ((F0 - F)/F) = log Kb + n log (CDV - CeO2 NPs)$$
(4)

K_b and n values are from the intercept and slope of the plot of log (F₀-F)/F versus log (CDV-CeO₂ NPs) (see Figures 16B, 17B and 18B). The values of K_b and n are given in (see Tables 1, 2 and 3). Since the value of n for all of the RNA and DNA systems was close to 1, it indicates that there is a binding site for the CDV-CeO₂ NPs on the RNA and DNA. For all of the RNA and DNA systems the K_b' values increase by temperature enhancing reveals

Increasing of the CDV-CeO₂ NPs

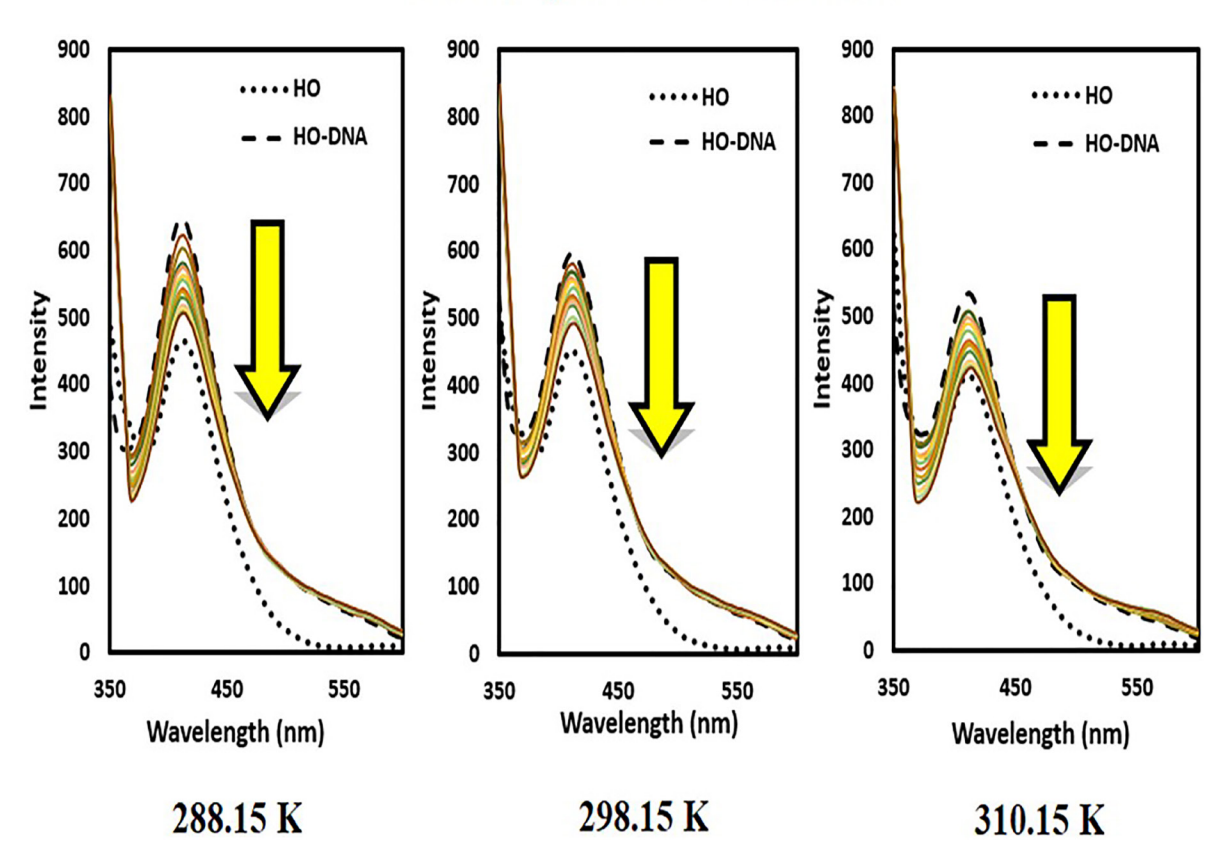


Figure 15: Fluorescence spectra of Hoechst + ct-DNA in the presence of CDV-CeO₂ NPs (2.44×10^{-5} to 2.59×10^{-4} g/mL), Ct-DNA = (1.76×10^{-4} M) $C_{Hoechst} = (5.00 \times 10^{-6}$ M).

that the CDV-CeO₂ NPs-nucleic acids complexes increase their stability on elevating temperature.

Thermodynamic parameters and interaction forces

To determine the thermodynamic binding parameters (ΔH^0 and ΔS^0), the researchers utilized the van't Hoff equation (Eq. 5) as follows:

$$Ln K_{b} = -\Delta H^{0}/RT + \Delta S^{0}/R$$
 (5)

The calculation of ΔH^0 and ΔS^0 can be achieved by using the slope and intercept of a linear van't Hoff plot. Gibbs free energy change (ΔG^0) is determined as:

$$\Delta G^0 = \Delta H^0 - T\Delta S^0 \tag{6}$$

Spontaneous binding is authenticated by the value of ΔG^0 that is negative. The enthalpy and entropy positive values (see Table 1, 2 and 3) suggest that hydrophobic interactions are taken part in the nucleic acids - CDV-CeO₂ NPs complex formation [62].

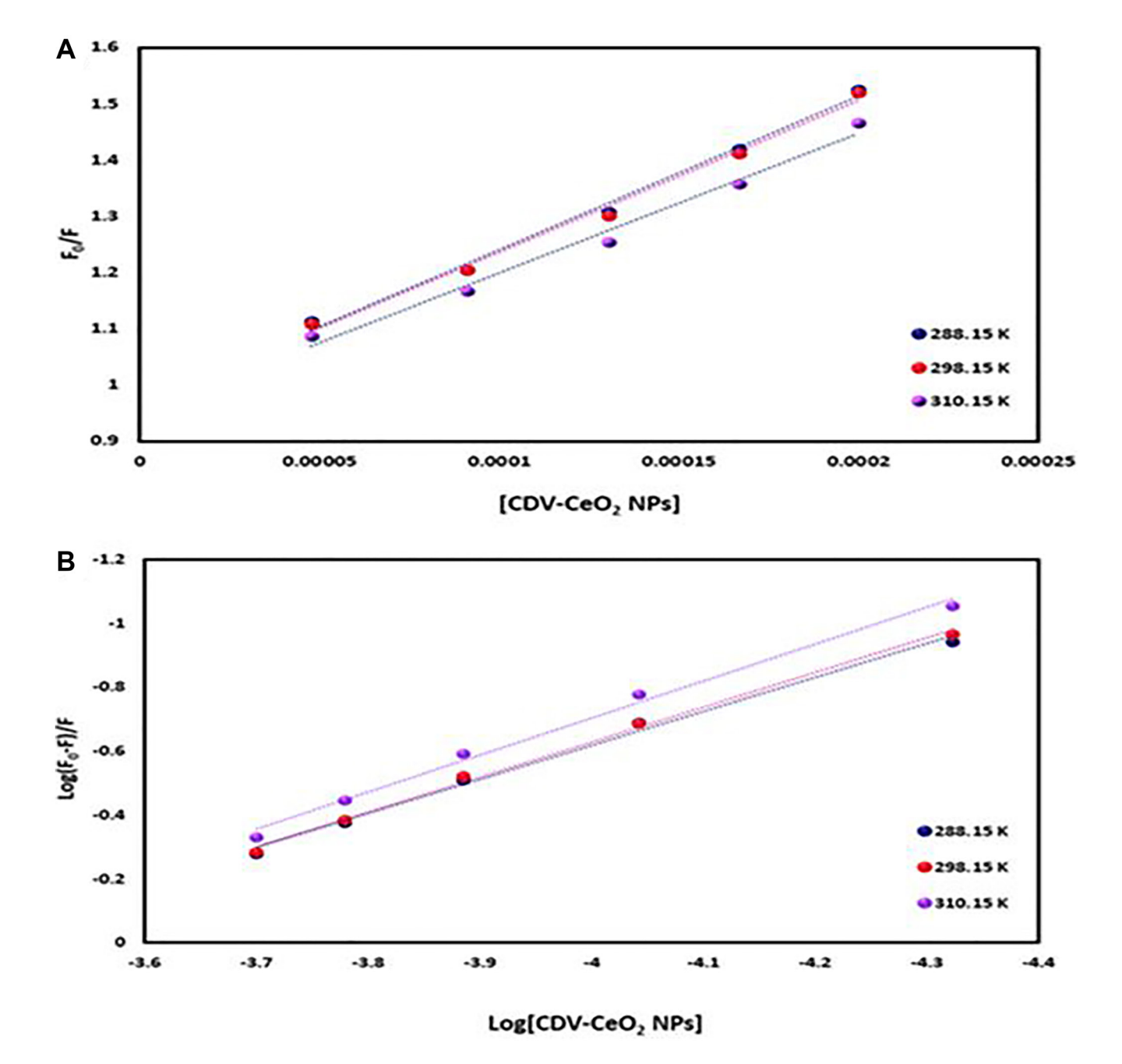


Figure 16: (A) Plot of F₀/F versus (CDV-CeO₂ NPs) for RNA–CDV-CeO₂ NPs system (RNA was labeled with AO). (B) Plot of log (F₀-F)/F versus log (CDV-CeO₂ NPs) for RNA–CDV-CeO₂ NPs system (RNA was labeled with AO).

MATERIALS AND METHODS

Materials

To synthesize CeO₂ nanoparticles using a green approach, Ce (NO₃)₃. 6H₂O salt was used. CDV was used for drug loading, while the MTT assay employed

3-(4, 5-dimethylthiazol-2-yl)-2, 5-diphenyl tetrazolium bromide (MTT), Fetal bovine serum, DMEM (Dulbecco Modified Eagles Medium), streptomycin, and penicillin. To investigate interactions, Tris- (hydroxymethyl)-aminomethane—hydrogen chloride, Hoechst 33258 (HO), Acridine orange (AO), Baker's yeast RNA sodium salt, and calf thymus DNA were provided from reputable

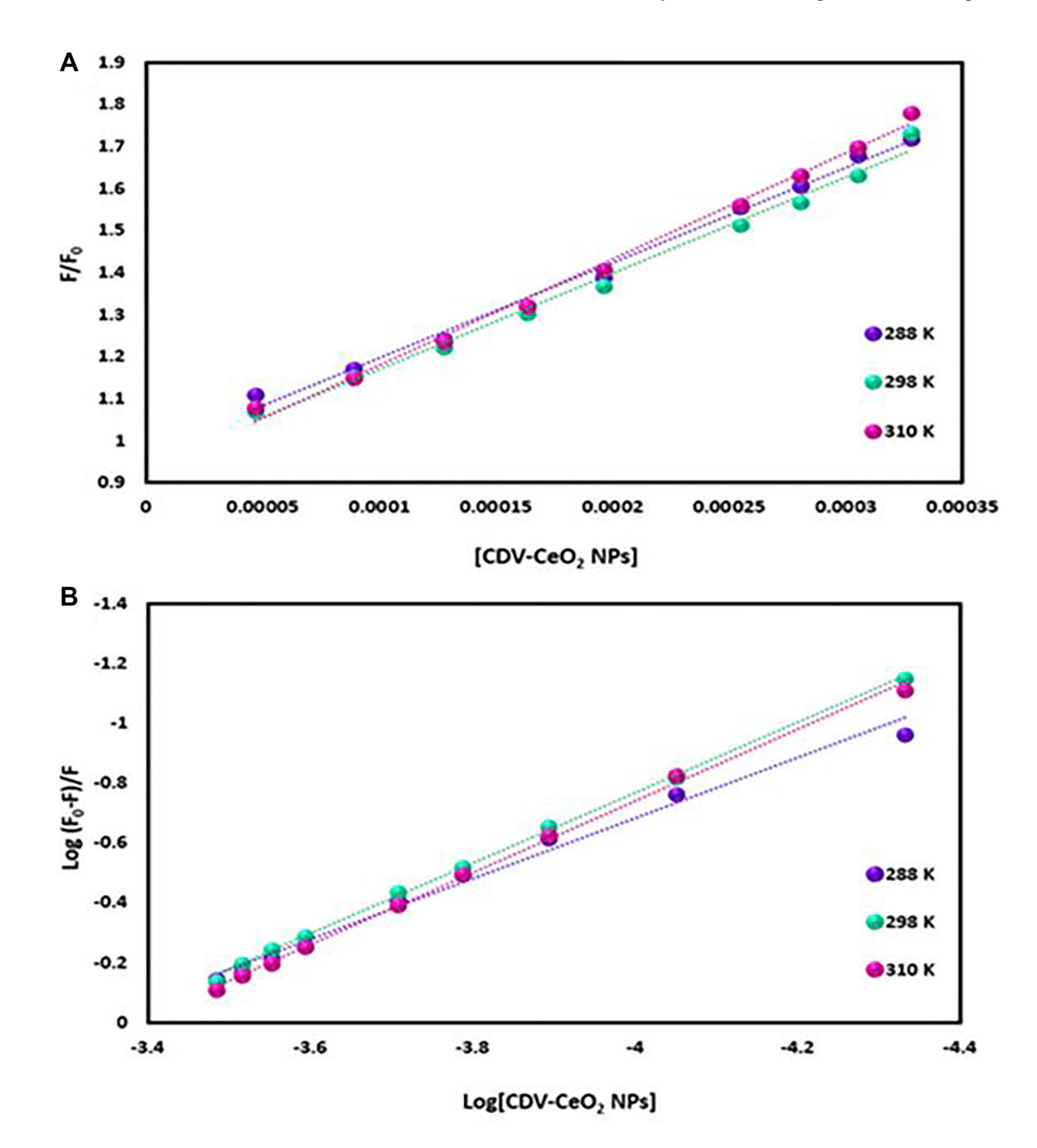


Figure 17: (A) Plot of F₀/F versus (CDV-CeO₂ NPs) for ct-DNA–CDV-CeO₂ NPs system (ct-DNA was labeled with AO). (B) Plot of log (F₀-F)/F versus log (CDV-CeO₂ NPs) for ct-DNA–CDV-CeO₂ NPs system (ct-DNA was labeled with AO).

companies. To create a Tris-HCl buffer solution with a pH of 7.4, Tris-(hydroxymethyl)aminomethane was dissolved in distilled water. For interaction experiments, the stock solution of RNA and DNA was prepared by dissolving a predetermined amount of pure RNA and DNA powder in Tris–HCl buffer. To assess the purity of the RNA and DNA solution, we measured the UV absorbance values at 260 and 280 nm (A_{260}/A_{280}), which yielded a value of 1.88. The HO and AO solution (1.00×10^{-3} M) was provided in distilled water. The CeO₂ nanoparticles solution with

a concentration of 1 mg/ml was provided by sonicating the NPs powder in distilled water for 10 minutes (refer to Figure 19B).

Preparation of the quince fruit (Cydonia oblonga) peel extract

Fruits of quince (*Cydonia oblonga*) were purchased and the peels of the fruit were taken (see Figure 19A). After that, the peels were cleaned by distilled water, then

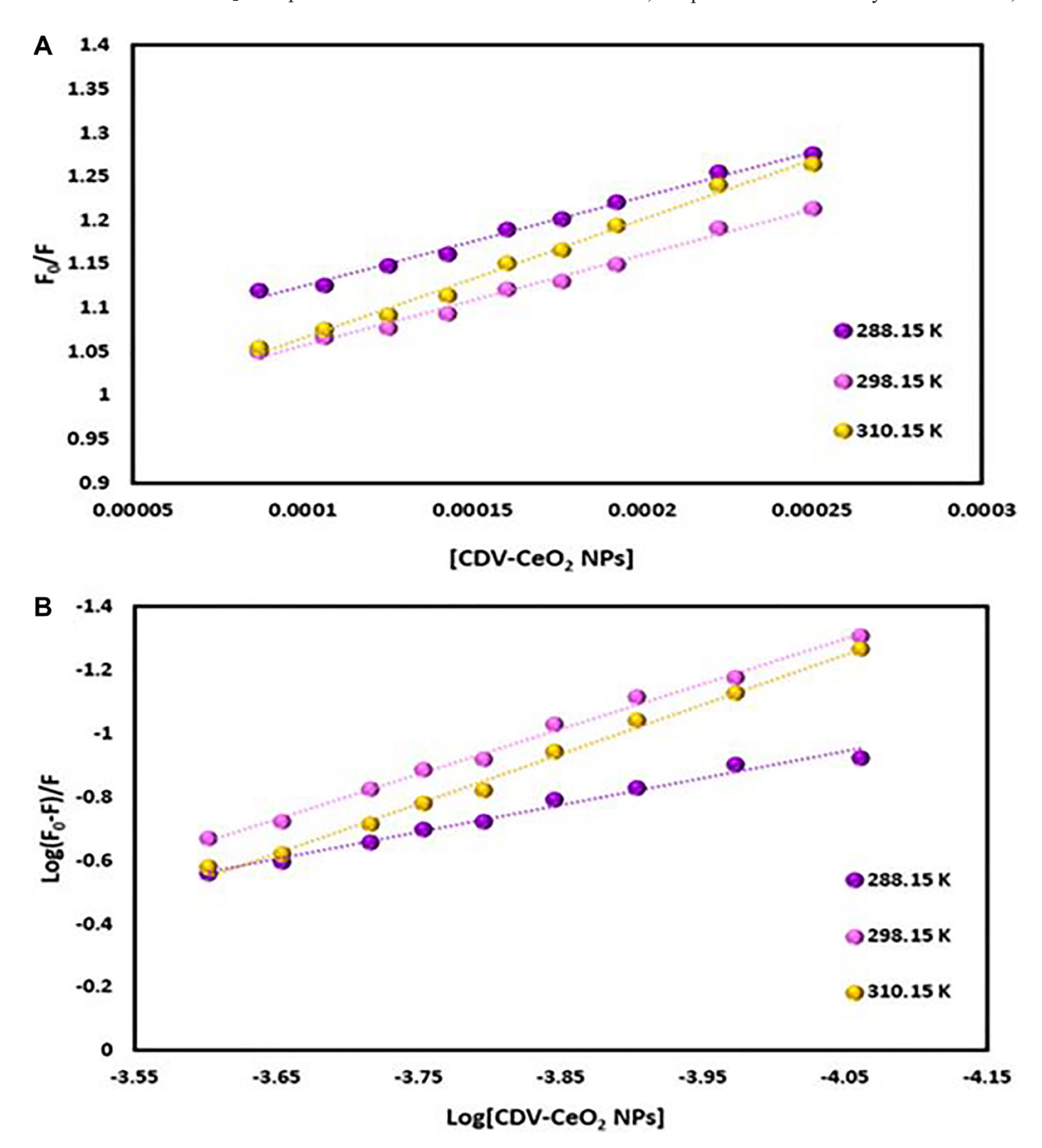


Figure 18: (A) Plot of F₀/F versus (CDV-CeO₂ NPs) for ct-DNA–CDV-CeO₂ NPs system (ct-DNA was labeled with HO). (B) Plot of log (F₀-F)/F versus log (CDV-CeO₂ NPs) for DNA–CDV-CeO₂ NPs system (ct-DNA was labeled with HO).

Table 1: Binding and thermodynamic parameters of the RNA-CDV-CeO₂ NPs system (RNA was labeled with AO)

T(K)	$\mathbf{K}_{\mathrm{sv}}(\mathbf{M}^{-1})^*$	$K_q (M^{-1}S^{-1})^*$	$\mathbf{K}_{b} (\mathbf{M}^{-1})^{*}$	n	ΔG ⁰ (kJmol ⁻¹)	ΔH ⁰ (kJmol ⁻¹)	$\Delta S^0 (Jmol^{-1}K^{-1})$
288.15	2.72×10^{3}	2.72×10^{11}	4.37×10^{3}	1.06	-19.99	21.62	144.42
298.15	2.69×10^{3}	2.69×10^{11}	5.31×10^{3}	1.09	-21.43		
310.15	2.48×10^3	2.48×10^{11}	8.25×10^3	1.15	-23.17		

 $^{^*}M = g/mL$.

Table 2: Binding and thermodynamic parameters of the ct-DNA-CDV-CeO₂ NPs system (ct-DNA was labeled with AO)

T(K)	$\mathbf{K}_{\mathrm{sv}}(\mathbf{M}^{-1})^*$	$K_q (M^{-1}S^{-1})^*$	$K_b (M^{-1})^*$	n	$\Delta G^{0}(kJmol^{-1})$	ΔH ⁰ (kJmol ⁻¹)	$\Delta S^0(Jmol^{-1}K^{-1})$
288.15	2.26×10^{3}	2.23×10^{11}	2.26×10^{3}	1.00	-18.99	53.41	251.26
298.15	2.28×10^3	$\textbf{2.28}\times\textbf{10}^{11}$	8.65×10^3	1.18	-21.50		
310.15	2.52×10^{3}	2.52×10^{11}	1.12×10^{4}	1.20	-24.52		

 $^{^*}M = g/mL.$

Table 3: Binding and thermodynamic parameters of the ct-DNA-CDV-CeO₂ NPs system (ct-DNA was labeled with HO)

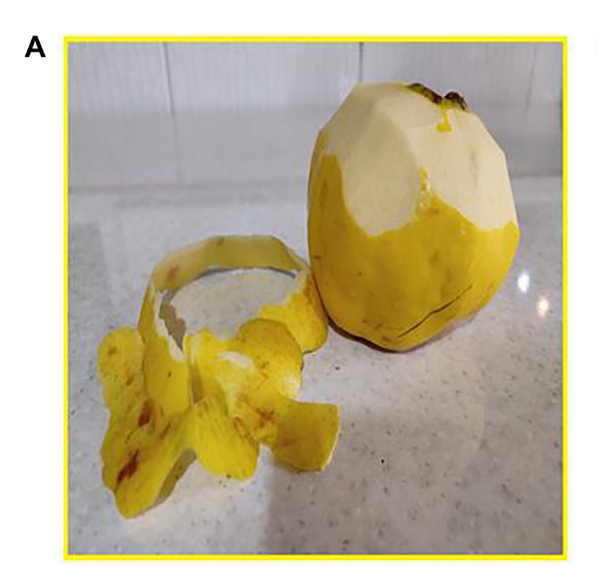
T(K)	$\mathbf{K}_{\mathrm{sv}}(\mathbf{M}^{-1})^*$	$K_q (M^{-1}S^{-1})^*$	$K_b (M^{-1})^*$	n	$\Delta G^{0}(kJmol^{-1})$	ΔH ⁰ (kJmol ⁻¹)	$\Delta S^0(Jmol^{-1}K^{-1})$
288.15	1.02×10^{3}	1.02×10^{11}	3.26×10^{2}	0.85	-36.02	197.01	736.74
298.15	1.04×10^{3}	1.04×10^{11}	2.85×10^{4}	1.42	-34.95		
310.15	1.36×10^{3}	1.36×10^{11}	1.19×10^{5}	1.56	-33.66		

^{*}M = g/mL Figure legends.

they were air-dried under shade for 5–7 days and grinded to obtain fine powdered form. The resulting powder was immersed in 100 mL of deionized water after grinding, and the mixture was boiled at 80°C for 30 minutes to obtain a concentrated yellowish-brown extract. After cooling to room temperature, the extract was filtered employing Whatman filter paper (41 pore size) and subsequently stored.

Preparation and characterization of NPs

To generate CeO₂ NPs using Cydonia oblonga peel extract, 3.72 g of Ce (NO₃)₃.6H₂O salt was added to the extract and gently stirred at 80°C for 20 hours. The process continued until the formation of a white precipitate. The precipitate gradually turned yellowish-



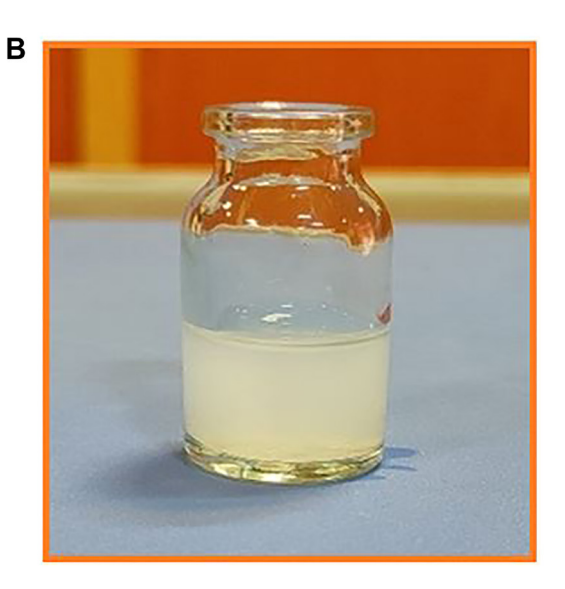


Figure 19: (A) The quince fruit and the peel of the quince fruit (B) digital photograph of CeO₂ NPs were dispersed in water.

brown on continuous stirring. The received precipitate was then calcined at 400°C for 2 hours, resulting in a yellow powder of CeO₂ NPs (loss of H₂O to form Ce(IV) oxide nanoparticles). Figure 20 shows a schematic diagram of the generation of CeO₂ NPs employing this method. The generation of NPs was confirmed through FT-IR, zeta potential, TEM, SEM-EDX, DLS, and ultraviolet-visible analysis.

Loading of CDV on the structure of the CeO₂ NPs

The CeO₂ nanoparticles solution (1 mg/ml) was initially sonicated in double-distilled water for 20 minutes at room temperature. Subsequently, the same solution was mixed with CDV solution (1 mg/mL) in equal volumes by stirring for 24 hours at room temperature. The resulting mixture was then centrifuged at 7000 rpm for 20 minutes to obtain CDV-CeO₂ nanoparticles. To assess the drug loading efficiency, the supernatant obtained from the centrifugation was subjected to spectrophotometry to determine the absorbance at 249 nm for unloaded drug. The calculation of the drug loading efficiency involved subtracting the quantity of unbound drug in the supernatant from the total amount of added drug. The standard curve equation was used to determine the drug loading efficiency, which was estimated using the following equation:

$$Loading efficiency = \frac{Total Drug - Unloaded Drug (in supernatant)}{Total Drug} \times 100$$
(7)

Cell culture conditions

To investigate the potential inhibitory effects of CDV, CeO_2 NPs, and CDV- CeO_2 NPs on cancer cell lines, MCF-7 cells were used. The cells were cultured in DMEM containing 200 mM L-glutamine, 10% fetal bovine serum (FBS), $100 \mu g/mL$ penicillin, and 10 mg/mL streptomycin. The cells were maintained under a 5% CO_2 atmosphere at $37^{\circ}C$

In vitro cytotoxicity (MTT assay)

The standard MTT assay was done to evaluate the anticancer potential of CDV, CeO₂ NPs, and CDV-CeO₂ NPs on MCF-7 cancer cells, following the methodology described in our previous studies [43, 63]. To begin, a predetermined number of cells (1 × 10⁴ cells) were seeded in a 96-well plate and incubated for 24 hours at 37°C. The cells were then treated with selected concentrations (2, 4, 8, 16, 32, and 64 μ g/mL) of CDV, CeO₂ NPs, and CDV-CeO₂ NPs for 24 hours. Next, MTT was added to each well and incubated for 4 hours. After incubation, 200 μ L of DMSO solution was added to each well and the plate was kept for 10 minutes. The plate absorbance was noted at 550–570 nm using an Elisa microplate reader.

Nucleic acids (DNA and RNA) binding affinity UV-Vis spectroscopy

The UV-visible spectra of RNA and DNA were noted alone and in the presence of CDV-CeO₂ NPs. The

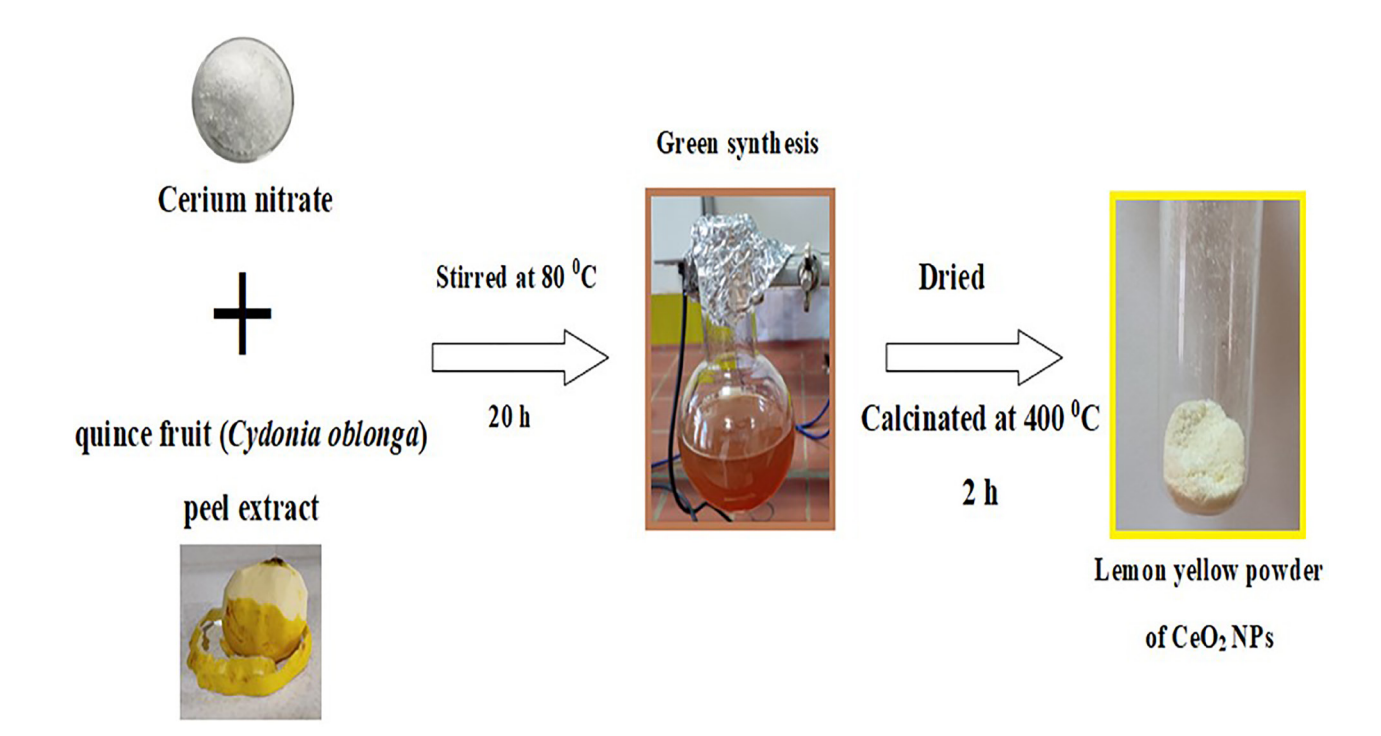


Figure 20: A schematic diagram for the generation of CeO₂ NPs using Cydonia oblonga peel extract.

measurement was taken across the wavelength range of 200 to 400 nm. A constant concentration of RNA and DNA (40 μ M) was titrated with varying concentrations (2.32 \times 10⁻⁵ to 1.76 \times 10⁻⁴ g/mL) of CDV-CeO₂ NPs, and baseline correction was performed using Tris-HCl buffer.

Fluorescence studies

Evaluating association mode

The groove binders (HO) and the intercalator fluorescence probe (AO) were utilized to elucidate the DNA-CDV-CeO₂ NPs and RNA-CDV-CeO₂ NPs interaction' mode. The CDV-CeO₂ NPs potential to displace probes from the DNA and RNA structure was assessed by performing the displacement experiment. To this end, the solution of AO, and HO $(5.00 \times 10^{-6} \,\mathrm{M})$ was titrated with DNA and RNA $(1.76 \times 10^{-4} \,\mathrm{M})$. Thereafter, CDV-CeO₂ NPs $(2.44 \times 10^{-5} \,\mathrm{to} \, 2.59 \times 10^{-4} \,\mathrm{g/mL})$ were transferred to the previous mixture. AO (noted from 640 to 730 nm by exciting at 502 nm), and HO (noted from, 350 to 650 nm by exciting at 340 nm).

CONCLUSIONS

The use of Cydonia oblonga peel extract in the green synthesis process provided an environmentally friendly method for producing CeO₂ NPs. These green-synthesized CeO₂ NPs were then functionalized with the anti-DNA virus agent CDV. The CDV-CeO2 NPs were characterized using various methods. This research indicates that the CDV-CeO₂ NPs show an inhibitory potential on cancerous cell line (MCF-7). Employing nucleic acids (DNA and RNA), the molecular recognition process and binding affinity of CDV-CeO2 NPs was deciphered by multi-spectroscopic methods. The evaluation of the fluorescence spectra and UV-visible absorption showed a strong association of the CDV-CeO₂ NPs with RNA/ DNA. Nonetheless, it is necessary to conduct a more thorough investigation to decipher the action mechanism before the assumption of a more significant role for the biosynthesized CDV-CeO₂ NPs for medicinal purposes.

AUTHOR CONTRIBUTIONS

Nahid Shahabadi: conceived and design the analysis; Saba Zendehcheshm: collected the data; Fatemeh Khademi: contributed data; Mohammad Mahdavi: contributed data.

ACKNOWLEDGMENTS

The authors would like to thank Razi University, Kermanshah, Iran, for providing laboratory facilities and technical support during the research process.

CONFLICTS OF INTEREST

Authors have no conflicts of interest to declare.

FUNDING

No funding was used for this paper.

REFERENCES

- Muthuvel A, Jothibas M, Manoharan C. Synthesis of copper oxide nanoparticles by chemical and biogenic methods: photocatalytic degradation and *in vitro* antioxidant activity, Nanotechnol. Environ Eng. 2020; 5:1–19. https://doi.org/10.1007/s41204-020-00078-w.
- Murugan R, Ravi G, Vijayaprasath G, Rajendran S, Thaiyan M, Nallappan M, Gopalan M, Hayakawa Y. Ni-CeO₂ spherical nanostructures for magnetic and electrochemical supercapacitor applications. Phys Chem Chem Phys. 2017; 19:4396–404. https://doi.org/10.1039/c6cp08281e. [PubMed]
- Milani ZM, Charbgoo F, Darroudi M. Impact of physicochemical properties of cerium oxide nanoparticles on their toxicity effects. Ceram Int. 2017; 43:14572–81. https://doi.org/10.1016/j.ceramint.2017.08.177.
- Li H, Wang G, Zhang F, Cai Y, Wang Y, Djerdj I. Surfactantassisted synthesis of CeO₂ nanoparticles and their application in wastewater treatment. RSC Adv. 2012; 2:12413–23. https://doi.org/10.1039/C2RA21590J.
- Hirst SM, Karakoti AS, Tyler RD, Sriranganathan N, Seal S, Reilly CM. Anti-inflammatory properties of cerium oxide nanoparticles. Small. 2009; 5:2848–56. https://doi.org/10.1002/smll.200901048. [PubMed]
- Dhall A, Self W. Cerium Oxide Nanoparticles: A Brief Review of Their Synthesis Methods and Biomedical Applications. Antioxidants (Basel). 2018; 7:97. https://doi.org/10.3390/antiox7080097. [PubMed]
- Charbgoo F, Ahmad MB, Darroudi M. Cerium oxide nanoparticles: green synthesis and biological applications. Int J Nanomedicine. 2017; 12:1401–13. https://doi.org/10.2147/IJN.S124855. [PubMed]
- Xu C, Qu X. Cerium oxide nanoparticle: a remarkably versatile rare earth nanomaterial for biological applications. NPG Asia Mater. 2014; 6:e90. https://doi.org/10.1038/am.2013.88.
- Celardo I, Pedersen JZ, Traversa E, Ghibelli L. Pharmacological potential of cerium oxide nanoparticles. Nanoscale. 2011; 3:1411–20. https://doi.org/10.1039/c0nr00875c. [PubMed]
- Celardo I, Traversa E, Ghibelli L. Cerium oxide nanoparticles: a promise for applications in therapy. J Exp Ther Oncol. 2011; 9:47–51. [PubMed]
- Tarnuzzer RW, Colon J, Patil S, Seal S. Vacancy engineered ceria nanostructures for protection from radiation-induced cellular damage. Nano Lett. 2005; 5:2573–77. https://doi.org/10.1021/nl052024f. [PubMed]
- 12. Niu J, Azfer A, Rogers LM, Wang X, Kolattukudy PE. Cardioprotective effects of cerium oxide nanoparticles in a transgenic murine model of cardiomyopathy.

- Cardiovasc Res. 2007; 73:549–59. https://doi.org/10.1016/j.cardiores.2006.11.031. [PubMed]
- 13. Schubert D, Dargusch R, Raitano J, Chan SW. Cerium and yttrium oxide nanoparticles are neuroprotective. Biochem Biophys Res Commun. 2006; 342:86–91. https://doi.org/10.1016/j.bbrc.2006.01.129. [PubMed]
- Charbgoo F, Ramezani M, Darroudi M. Bio-sensing applications of cerium oxide nanoparticles: Advantages and disadvantages. Biosens Bioelectron. 2017; 96:33–43. https://doi.org/10.1016/j.bios.2017.04.037. [PubMed]
- Darroudi M, Hoseini SJ, Oskuee RK, Hosseini HA, Gholami L, Gerayli S. Food-directed synthesis of cerium oxide nanoparticles and their neurotoxicity effects. Ceram Int. 2014; 40:7425–30. https://doi.org/10.1016/j.ceramint.2013.12.089.
- Darroudi M, Sarani M, Oskuee RK, Zak AK, Amiri MS. Nanoceria: Gum mediated synthesis and *in vitro* viability assay. Ceram Int. 2014; 40:2863–68. https://doi.org/10.1016/j.ceramint.2013.10.026.
- 17. Periyat P, Laffir F, Tofail S, Magner E. A facile aqueous sol–gel method for high surface area nanocrystalline CeO₂. RSC adv. 2011; 1:1794–98. https://doi.org/10.1039/C1RA00524C.
- Yu R, Yan L, Zheng P, Chen J, Xing X. Controlled synthesis of CeO₂ flower-like and well-aligned nanorod hierarchical architectures by a phosphate-assisted hydrothermal route. J Phys Chem C. 2008; 112:19896–900. https://doi.org/10.1021/jp806092q.
- Yao H, Wang Y, Luo G. A size-controllable precipitation method to prepare CeO₂ nanoparticles in a membrane dispersion microreactor. Ind Eng Chem. 2017; 56:4993–99. https://doi.org/10.1021/acs.iecr.7b00289.
- Devaraju MK, Yin S, Sato T. Morphology control of cerium oxide particles synthesized via a supercritical solvothermal method. ACS Appl Mater Interfaces. 2009; 1:2694–8. https://doi.org/10.1021/am900574m. [PubMed]
- Supakanapitak S, Boonamnuayvitaya V, Jarudilokkul S. Synthesis of nanocrystalline CeO₂ particles by different emulsion methods. Mater Charact. 2012; 67:83–92. https://doi.org/10.1016/J.MATCHAR.2012.02.018.
- Bakkiyaraj R, Bharath G, Ramsait KH, Abdel-Wahab A, Alsharaeh EH, Chen SM, Balakrishnan M. Solution combustion synthesis and physico-chemical properties of ultrafine CeO₂ nanoparticles and their photocatalytic activity. RSC adv. 2016; 67:51238–45. https://doi.org/10.1039/C6RA00382F.
- Goharshadi EK, Samiee S, Nancarrow P. Fabrication of cerium oxide nanoparticles: characterization and optical properties. J Colloid Interface Sci. 2011; 356:473–80. https://doi.org/10.1016/j.jcis.2011.01.063. [PubMed]
- Krishnan A, Sreeremya TS, Murray E, Ghosh S. One-pot synthesis of ultra-small cerium oxide nanodots exhibiting multi-colored fluorescence. J Colloid Interface Sci. 2013; 389:16–22. https://doi.org/10.1016/j.jcis.2012.09.009. [PubMed]

- Maensiri S, Masingboon C, Laokul P, Jareonboon W, Promarak V, Anderson P, Seraphin S. Egg white synthesis and photoluminescence of platelike clusters of CeO₂ nanoparticles. Cryst Growth Des. 2007; 7:950–55. https://doi.org/10.1021/cg0608864.
- Khan SA, Asiri AM, Alamry KA, El-Daly SA, Zayed MA. Eco-friendly synthesis and *in vitro* antibacterial activities of some novel chalcones. Bioorg Khim. 2013; 39:353–57. https://doi.org/10.1134/s1068162013030072. [PubMed]
- 27. Sajid SM, Zubair M, Waqas M, Nawaz M, Ahmad Z. A review on quince (Cydonia oblonga): A useful medicinal plant. Glob Vet. 2015; 14:517–24.
- 28. Duron M, Decourtye L, Druart P. Quince (Cydonia oblonga Mill.). Trees II. 1989; 42–58. https://doi.org/10.1007/978-3-642-61535-1 4.
- Gironés-Vilaplana A, Baenas N, Villaño D, Moreno DA. Iberian-American fruits rich in bioactive phytochemicals for nutrition and health. LIMENCOP SL: Alicante, Spain. 2014.
- Babashpour-Asl M, Piryaei M. Free radical scavengering and phenolic compounds of peel and pulp of quince. Int J Hortic Sci Technol. 2021; 8:91–101. https://doi.org/10.22059/ijhst.2020.285851.308.
- Ashraf MU, Muhammad G, Hussain MA, Bukhari SN. Cydonia oblonga M., A Medicinal Plant Rich in Phytonutrients for Pharmaceuticals. Front Pharmacol. 2016; 7:163. https://doi.org/10.3389/fphar.2016.00163. [PubMed]
- Stojanović BT, Mitić SS, Stojanović GS, Mitić MN, Kostić DA, Paunović DĐ, Arsić BB, Pavlović AN. Phenolic profiles and metal ions analyses of pulp and peel of fruits and seeds of quince (Cydonia oblonga Mill.). Food Chem. 2017; 232:466–75. https://doi.org/10.1016/j.foodchem.2017.04.041. [PubMed]
- Silva BM, Andrade PB, Ferreres F, Domingues AL, Seabra RM, Ferreira MA. Phenolic profile of quince fruit (Cydonia oblonga Miller) (pulp and peel). J Agric Food Chem. 2002; 50:4615–8. https://doi.org/10.1021/jf0203139. [PubMed]
- Oliveira AP, Pereira JA, Andrade PB, Valentão P, Seabra RM, Silva BM. Phenolic profile of Cydonia oblonga Miller leaves. J Agric Food Chem. 2007; 55:7926–30. https://doi.org/10.1021/jf0711237. [PubMed]
- Mirzaei-Kalar Z, Yavari A, Jouyban A. Increasing DNA binding affinity of doxorubicin by loading on Fe₃O₄ nanoparticles: A multi-spectroscopic study. Spectrochim Acta A Mol Biomol Spectrosc. 2020; 229:117985. https://doi.org/10.1016/j.saa.2019.117985. [PubMed]
- Kausar S, Said Khan F, Ishaq Mujeeb Ur Rehman M, Akram M, Riaz M, Rasool G, Hamid Khan A, Saleem I, Shamim S, Malik A. A review: Mechanism of action of antiviral drugs. Int J Immunopathol Pharmacol. 2021; 35:20587384211002621. https://doi.org/10.1177/20587384211002621. [PubMed]
- 37. Mertens B, Nogueira T, Stranska R, Naesens L, Andrei G, Snoeck R. Cidofovir is active against human papillomavirus

- positive and negative head and neck and cervical tumor cells by causing DNA damage as one of its working mechanisms. Oncotarget. 2016; 7:47302–18. https://doi.org/10.18632/oncotarget.10100. [PubMed]
- Hadaczek P, Ozawa T, Soroceanu L, Yoshida Y, Matlaf L, Singer E, Fiallos E, James CD, Cobbs CS. Cidofovir: a novel antitumor agent for glioblastoma. Clin Cancer Res. 2013; 19:6473–83. https://doi.org/10.1158/1078-0432.CCR-13-1121. [PubMed]
- 39. Turel I, Kljun J. Interactions of metal ions with DNA, its constituents and derivatives, which may be relevant for anticancer research. Curr Top Med Chem. 2011; 11:2661–87. https://doi.org/10.2174/156802611798040787. [PubMed]
- 40. Wang Y, Rando RR. Specific binding of aminoglycoside antibiotics to RNA. Chem Biol. 1995; 2:281–90. https://doi.org/10.1016/1074-5521(95)90047-0. [PubMed]
- Elahi B, Mirzaee M, Darroudi M, Oskuee RK, Sadri K, Amiri MS. Preparation of cerium oxide nanoparticles in Salvia Macrosiphon Boiss seeds extract and investigation of their photo-catalytic activities. Ceram Int. 2019; 45:4790– 97. https://doi.org/10.1016/j.ceramint.2018.11.173.
- Kumar CG, Poornachandra Y. Biodirected synthesis of Miconazole-conjugated bacterial silver nanoparticles and their application as antifungal agents and drug delivery vehicles. Colloids Surf B Biointerfaces. 2015; 125:110–119. https://doi.org/10.1016/j.colsurfb.2014.11.025. [PubMed]
- 43. Dutta T, Ghosh NN, Das M, Adhikary R, Mandal V, Chattopadhyay AP. Green synthesis of antibacterial and antifungal silver nanoparticles using Citrus limetta peel extract: Experimental and theoretical studies. J Environ Chem Eng. 2020; 8:104019. https://doi.org/10.1016/j.jece.2020.104019.
- Buszewski B, Rafifska K, Pomastowski P, Walczak J, Rogowska A. Novel aspects of silver nanoparticles functionalization, Colloids Surf. A Physicochem Eng Asp. 2016; 506:170–78. https://doi.org/10.1016/j.colsurfa.2016.05.058.
- 45. Parvathya S, Venkatramanb BR. *In vitro* antibacterial and anticancer potential of CeO₂ nanoparticles prepared by coprecipitation and green synthesis method. J Nanosci Curr Res. 2017; 2:1–9.
- 46. Bharathi D, Ranjithkumar R, Chandarshekar B, Bhuvaneshwari V. Preparation of chitosan coated zinc oxide nanocomposite for enhanced antibacterial and photocatalytic activity: As a bionanocomposite. Int J Biol Macromol. 2019; 129:989–96. https://doi.org/10.1016/j.ijbiomac.2019.02.061. [PubMed]
- Shahabadi N, Zendehcheshm S, Khademi F, Rashidi K, Chehri K. Green synthesis of Chloroxine-conjugated silver nanoflowers: promising antimicrobial activity and *in vivo* cutaneous wound healing effects. J Environ Chem Eng. 2021; 9:105215. https://doi.org/10.1016/j.jece.2021.105215.
- 48. Arumugam A, Karthikeyan C, Haja Hameed AS, Gopinath K, Gowri S, Karthika V. Synthesis of cerium oxide

- nanoparticles using Gloriosa superba L. leaf extract and their structural, optical and antibacterial properties. Mater Sci Eng C Mater Biol Appl. 2015; 49:408–15. https://doi.org/10.1016/j.msec.2015.01.042. [PubMed]
- 49. Ahmed HE, Iqbal Y, Aziz MH, Atif M, Batool Z, Hanif A, Yaqub N, Farooq W, Ahmad S, Fatehmulla A. Green synthesis of CeO₂ nanoparticles from the Abelmoschus esculentus extract: evaluation of antioxidant, anticancer, antibacterial, and wound-healing activities. Molecules. 2021; 6:4659. https://doi.org/10.3390/molecules26154659.
- Kannan SK, Sundrarajan M. A green approach for the synthesis of a cerium oxide nanoparticle: characterization and antibacterial activity. Int J Nanosci. 2014; 13:1450018. https://doi.org/10.1142/S0219581X14500185.
- Phoka S, Laokul P, Swatsitang E, Promarak V, Seraphin S, Maensiri S. Synthesis, structural and optical properties of CeO₂ nanoparticles synthesized by a simple polyvinyl pyrrolidone (PVP) solution route. Mater Chem Phys. 2009; 115:423–28. https://doi.org/10.1016/j.matchemphys.2008.12.031.
- Sonvico F, Colombo G, Gallina L, Bortolotti F, Rossi A, McInnes CJ, Massimo G, Colombo P, Scagliarini A. Therapeutic paint of cidofovir/sucralfate gel combination topically administered by spraying for treatment of orf virus infections. AAPS J. 2009; 11:242–49. https://doi.org/10.1208/s12248-009-9101-8. [PubMed]
- Shahabadi N, Falsafi M, Mansouri K. Improving antiproliferative effect of the anticancer drug cytarabine on human promyelocytic leukemia cells by coating on Fe3O4@ SiO₂ nanoparticles. Colloids Surf B Biointerfaces. 2016; 141:213–22. https://doi.org/10.1016/j.colsurfb.2016.01.054. [PubMed]
- Karampour F. Green Synthesis of γ-Fe2O3@ SiO2 Coated by an Antiviral Drug Cidofovir as New Magnetic Nanoparticles: Synthesis, Characterization and Cytotoxicity Properties. IJABBR. 2024; 12:357–70. https://doi.org/10.48309/ijabbr.2024.2029303.1514.
- 55. Shahabadi N, Shiri F, Norouzibazaz M, Falah A. Disquisition on the interaction of ibuprofen-Zn(II) complex with calf thymus DNA by spectroscopic techniques and the use of Hoechst 33258 and Methylene blue dyes as spectral probes. Nucleosides Nucleotides Nucleic Acids. 2018; 37:125–46. https://doi.org/10.1080/15257770.2017.1400048. [PubMed]
- Shahabadi N, Zendehcheshm S, Khademi F. Exploring the ct-DNA and plasmid DNA binding affinity of the biogenic synthesized Chloroxine-conjugated silver nanoflowers: Spectroscopic and gel electrophoresis methods. Process Biochem. 2022; 121:360–70. https://doi.org/10.1016/j.procbio.2022.07.024.
- 57. Shahabadi N, Zendehcheshm S. Evaluation of ct-DNA and HSA binding propensity of antibacterial drug chloroxine: Multi-spectroscopic analysis, atomic force microscopy and docking simulation. Spectrochim Acta A Mol Biomol Spectrosc. 2020; 230:118042. https://doi.org/10.1016/j.saa.2020.118042. [PubMed]

- Shahabadi N, Zendehcheshm S, Momeni BZ, Abbasi R. Antiproliferative activity and human serum albumin binding propensity of (SnMe2Cl2 (bu2bpy)): multi-spectroscopic analysis, atomic force microscopy, and computational studies. J Coord Chem. 2020; 73:1349–76. https://doi.org/10.1080/00958972.2020.1775821.
- Shahabadi N, Zendehcheshm S, Mahdavi M. Exploring the In-Vitro Antibacterial Activity and Protein (Human Serum Albumin, Human Hemoglobin and Lysozyme) Interaction of Hexagonal Silver Nanoparticle Obtained from Wood Extract of Wild Cherry Shrub. ChemistrySelect. 2023; 8:e202204672. https://doi.org/10.1002/slct.202204672.
- Shahabadi N, Zendehcheshm S. Interaction of human hemoglobin (HHb) and cytochrome c (Cyt c) with biogenic chloroxine-conjugated silver nanoflowers: spectroscopic and molecular docking approaches. J Biomol Struct Dyn. 2022; 40:8913–24. https://doi.org/10.1080/07391102.2021 .1919555. [PubMed]

- Shahabadi N, Momeni BZ, Zendehcheshm S. Studies on the Interaction of [SnMe₂Cl₂(bu₂bpy)] Complex with ct-DNA Using Multispectroscopic, Atomic Force Microscopy (AFM) and Molecular Docking. Nucleosides Nucleotides Nucleic Acids. 2019; 38:157–82. https://doi.org/10.1080/15257770.2018.1506885. [PubMed]
- Shahabadi N, Zendehcheshm S, Khademi F. Green Synthesis, in vitro Cytotoxicity, Antioxidant Activity and Interaction Studies of CuO Nanoparticles with DNA, Serum Albumin, Hemoglobin and Lysozyme. ChemistrySelect. 2022; 7:e202202916. https://doi.org/10.1002/slct.202202916.
- 63. Shahabadi N, Zendehcheshm S, Khademi F. Selenium nanoparticles: Synthesis, *in-vitro* cytotoxicity, antioxidant activity and interaction studies with ct-DNA and HSA, HHb and Cyt c serum proteins. Biotechnol Rep (Amst). 2021; 30:e00615. https://doi.org/10.1016/j.btre.2021.e00615. [PubMed]